OCA-B promotes pathogenic maturation of stem-like CD4+ T cells and autoimmune demyelination

Erik P. Hughes[1,3], Amber R. Syage[1,3], Elnaz Mirzaei Mehrabad[2,3,4], Thomas E. Lane[5], Benjamin T. Spike[2,3], Dean Tantin[1,3]

[1]Department of Pathology, University of Utah School of Medicine, Salt Lake City, UT, USA. [2]Department of Oncological Sciences, University of Utah School of Medicine, Salt Lake City, UT, USA. [3]Huntsman Cancer Institute, University of Utah School of Medicine, Salt Lake City, UT, USA. [4]School of Computing, University of Utah, Salt Lake City, UT, USA. [5]Department of Neurobiology and Behavior, School of Biological Sciences, University of California, Irvine, CA, USA.

Correspondence to Dean Tantin:
Huntsman Cancer Institute, 2000 Circle of Hope, Research South Room 3707
Salt Lake City, UT 84112-5550
dean.tantin@path.utah.edu
801-587-3035

Short title: OCA-B promotes CD4+ T cell mediated demyelinating disease

Keywords Adaptive immunity; OCA-B/Bob1/Pou2af1; autoimmunity; multiple sclerosis; experimental autoimmune encephalomyelopathy; CD4+ T cells; relapsing-remitting

Conflicts of interest statement: The authors have declared that no conflict of interest exists

Words in abstract: 195
Words main text: 11,124
Total main display items: 6

Abstract

Stem-like T cells selectively contribute to autoimmunity, but the activities that promote their pathogenicity are incompletely understood. Here, we identify the transcription coregulator OCA-B as a driver of the pathogenic maturation of stem-like $CD4^+$ T cell to promote autoimmune demyelination. Using a human multiple sclerosis (MS) patient dataset, we show that *POU2AF1*, the gene encoding OCA-B, is elevated in $CD4^+$ T cells from secondary-progressive MS patient lesions. We show that T cell-intrinsic OCA-B loss protects mice from experimental autoimmune encephalomyelitis (EAE) while preserving responses to viral CNS infection. In EAE models driven by antigen reencounter, OCA-B deletion nearly eliminates CNS infiltration, proinflammatory cytokine production and clinical disease. CNS OCA-B-expressing $CD4^+$ T of mice with EAE express an encephalitogenic gene program and preferentially confer disease. In a relapsing-remitting EAE model, OCA-B loss protects mice specifically at relapse. During remission, OCA-B promotes the expression of *Tcf7*, *Slamf6*, and *Sell* in proliferating CNS T cell populations. At relapse timepoints, OCA-B loss results in both the accumulation of an immunomodulatory $CD4^+$ T cell population expressing *Ccr9* and *Bach2*, and loss of pro-inflammatory gene expression from Th17 cells. These results identify OCA-B as a driver of pathogenic $CD4^+$ T cells.

Introduction

2.8 million individuals worldwide suffer from multiple sclerosis (MS), with almost 1 million cases in the United States (1). Despite recent advances, the development of new therapies that block MS while sparing immunosurveillance mechanisms needed to prevent infection and viral recrudescence remains a critical goal. Genome-wide association studies (GWAS) identify the *HLA* loci as the most important determinant of MS pathogenesis, emphasizing the impact of T cells (2, 3). The association with the major histocompatibility complex (MHC) class II locus in particular indicates that myelin-specific $CD4^+$ T cells are key regulators of disease.

The predominant preclinical model of MS is experimental autoimmune encephalomyelitis (EAE), in which laboratory animals are immunized with myelin proteins or peptides to activate antigen-specific $CD4^+$ T cells that infiltrate the central nervous system (CNS) and mediate disease. EAE within the C57BL/6 mouse background establishes chronic disease. In these models, Th1 and Th17 effector $CD4^+$ T cell subsets are pathogenetic mediators (4, 5). After accessing the CNS, these cells promote neuroinflammation through the secretion of interferon-gamma (IFNγ), interleukin-17 (IL-17), granulocyte macrophage stimulating-factor (GM-CSF) and other inflammatory mediators and chemoattractants that recruit the cell types responsible for driving demyelination (6–8).

Myelin-reactive T cells from the blood of MS patients show stem/memory-like properties, with reduced need for co-stimulation, suggesting signs of previous activation (9–12). Consistent with these findings, autoreactive and bystander memory-phenotype $CD4^+$ T cells preferentially transfer demyelinating disease in mouse models (13–15). While these studies have identified vital $CD4^+$ T cell populations in EAE, further research on the mechanisms sustaining these populations and driving their pathogenic activity is required to develop more precise therapies.

Oct1, a POU domain transcription factor encoded by *Pou2f1*, has been linked to autoimmune disease. GWAS studies have identified Oct1 binding site polymorphisms that associate with a predisposition for autoimmune diseases, including MS (16–19). In $CD4^+$ T cells, Oct1 promotes the development of both $CD4^+$ memory (20) and EAE pathogenesis and demyelination (21). In contrast, Oct1 loss preserves immune responses to the neurotrophic viral infection (21). These observations highlight a promising pathway which when targeted may limit autoimmune CNS demyelination without the broad immune suppression elicited by many current therapeutics. However, Oct1 itself is widely expressed and regulates both embryonic development and somatic stem cell function (22–24), making it a poor therapeutic target.

The lymphoid-restricted transcription cofactor OCA-B regulates transcription by docking with Oct1, and in B cells an additional related factor, Oct2 (25). In contrast to Oct1, OCA-B whole-

82 body knockouts are viable and fertile (26). Polymorphisms in the *Ocab* (*Pou2af1*) locus are
83 associated with autoimmune diseases, including MS (27, 28). Although its expression is 50-100
84 fold lower in T cells compared to B cells (29), targeting either OCA-B by genetic deletion in T cells
85 or its downstream pathways with a membrane-permeable peptide mimic suppresses type-1
86 diabetes (30). OCA-B interacts with target genes such as *Il2, Ifng, Il21, Csf2 (Gmcsf), Tnfrsf4*
87 *(Ox40), Icos* and *Ctla4*, but is dispensable for their expression following primary activation of T
88 cells. Instead, OCA-B regulates these targets under a narrow range of conditions, for example
89 following secondary stimulation in culture (20). Many of these targets are directly implicated in
90 MS pathogenesis (6–8, 31–37). OCA-B controls expression of *Tbx21* (*Tbet*), which encodes a
91 key regulator of Th1 effector responses, but also promotes Th17 differentiation and interacts with
92 RORγt, a master regulator of Th17 cells (20, 38, 39). In the context of MS, the only prior OCA-B
93 work used whole body knockouts and showed partial protection in chronic C57BL/6 EAE models
94 (39). Cumulatively, these findings indicate that OCA-B plays poorly defined but possibly significant
95 roles in MS pathogenesis.
96 Here, we show that OCA-B within the T cell compartment drives EAE by promoting
97 pathogenic maturation of stem-like $CD4^+$ T cells. In C57BL/6 mice, T cell OCA-B loss significantly
98 protects mice from chronic EAE while preserving responses to the neurotrophic coronavirus
99 JHMV. Using Th1 and Th17 passive transfer assays in which reactive T cells are primed with
100 antigen in donor mice and in polarizing culture, and reencounter antigen in naïve recipients, we
101 show that OCA-B is critical for the infiltration of pathogenic cells into the CNS and the
102 manifestation of clinical disease. Using an OCA-B reporter mouse, we find that OCA-B expressing
103 $CD4^+$ T cells taken from MOG peptide primed mice preferentially display pathogenic stem-like
104 gene expression and preferentially transfer demyelinating disease, highlighting OCA-B as a
105 marker and promoter of encephalitogenic autoimmune $CD4^+$ T cell activity. Intriguingly, T cell
106 conditional OCA-B knockout in EAE models on the autoimmune-prone non-obese diabetic (NOD)
107 background, which develop relapsing-remitting disease (40), specifically protects against relapse.
108 Single-cell transcriptomic analysis of $CD3\varepsilon^+$, CNS-infiltrating T cells at remission and relapse
109 indicates that OCA-B promotes disease relapse through control of stem-like T cell populations,
110 driving them to pathogenic Th17 differentiation. Cumulatively, these findings mark OCA-B as a
111 critical mediator of the pathogenic maturation of autoreactive T cells, and a promising potential
112 therapeutic target.

113 Results

114 *Elevated expression of the gene encoding OCA-B in CD4+ T cells from secondary-progressive*
115 *human MS lesions.* To determine if *OCAB* (*POU2AF1*) is elevated in human MS samples, we
116 mined high-throughput single-nucleus RNA-seq data of glial and immune cells (including T cells)
117 from a recent study using single-nucleus RNA-seq to evaluate gene expression in brain tissue
118 from 54 MS patients and 26 non-MS controls (41). The number of relapsing-remitting (RRMS)
119 samples was small. The N=1 RRMS sample showed far higher *POU2AF1* expression compared
120 to CTR (Figure 1A). There were more primary-progressive (PPMS) samples, and interestingly
121 only one sample showed significant expression, perhaps reflecting imperfections in diagnoses.
122 Most dramatically, a subset of secondary-progressive (SPMS) samples showed highly elevated
123 OCA-B expression (Figure 1A). We then reclustered $CD4^+$ cell nuclei from this dataset. Uniform
124 Manifold Approximation and Projection (UMAP) feature plots revealed that the elevated
125 *POU2AF1* found in T cell nuclei found from SPMS patients was confined to one specific cluster
126 that also expresses the pathogenic marker *IL1R1* (Figure 1B).

127

128 *OCA-B promotes chronic EAE in C57BL/6 mice.* To understand the impact of OCA-B in T cell
129 mediated autoimmunity, we utilized an *Ocab* conditional knockout allele crossed to the CD4-Cre
130 driver which efficiently deletes OCA-B in T cells (30). We induced EAE in C57BL/6 female
131 $Ocab^{fl/fl}$;CD4-Cre mice and littermate $Ocab^{fl/fl}$ controls through subcutaneous (s.c.) injection of
132 myelin oligodendrocyte glycoprotein $(MOG)_{35\text{-}55}$ peptide in Complete Freund's Adjuvant (CFA)
133 followed by intraperitoneal (i.p.) injections of *Bordetella pertussis* toxin. $Ocab^{fl/fl}$;CD4-Cre mice
134 showed reduced chronic EAE clinical scores and weight loss compared to $Ocab^{fl/fl}$ littermate
135 controls (Figure 1C-D). Spinal cords were taken at peak disease (day 15) for immunofluorescence
136 and histological analysis. Myelin basic protein (MBP) immunofluorescence showed a significant
137 decrease in demyelinated white matter in spinal sections from $Ocab^{fl/fl}$;CD4-Cre mice compared
138 to littermate $Ocab^{fl/fl}$ controls while DAPI showed simultaneously decreased immune cell
139 infiltration (Figure 1E-F). $Ocab^{fl/fl}$;CD4-Cre mice also showed a significant decrease in
140 demyelination as measured by luxol fast blue (LFB) in combination with hematoxylin and eosin
141 (H&E) staining (Supplemental Figure 1A-B). Flow cytometric profiling at peak disease showed
142 decreased $CD4^+$ T cell CNS infiltration using $Ocab^{fl/fl}$;CD4-Cre mice, however no differences in
143 other infiltrating cell populations or in the relative frequencies of the proinflammatory cytokines
144 IFNy, IL-17, GM-CSF, or CD44 were observed (Figure 1G-H and Supplemental Figure 1C-H). We
145 studied MOG-specific $CD4^+$ T cells using the MHC class II I-A^b $MOG_{38\text{-}49}$ tetramers. At peak

146 disease, *Ocab*$^{fl/fl}$;CD4-Cre mice showed a trending reduction in MOG tetramer-specific cell
147 frequency (p=0.055) and a significant reduction in numbers (p=0.003) compared to controls
148 (Figure 1I-J). These results indicate that the protection conferred by OCA-B loss in T cells is
149 marked by modest decreases in MOG-specific CD4$^+$ T cells within the CNS, resulting in fewer
150 pathogenic T cells driving demyelination.

151 *OCA-B is essential for EAE mediated by adoptive transfer of Th1- and Th17-polarized T*
152 *cells.* MS is driven by autoreactive CD4$^+$ Th1 and Th17 cells within the CNS that recruit CD8$^+$ T
153 cells, macrophages, microglia and neutrophils, which together mediate white-matter damage (42).
154 To investigate the impact of OCA-B on autoimmune Th1 and Th17 populations, we used adoptive
155 transfer EAE models with female *Ocab*$^{fl/fl}$;CD4-Cre and *Ocab*$^{fl/fl}$ littermate controls. Mice were
156 primed with MOG_{35-55} in CFA for 14 days. Following MOG priming, CD4$^+$ T cells were purified
157 from the lymph nodes of primed experimental or control donors. No differences between
158 genotypes in CD4$^+$ T cell viability, count, or effector cytokine (IFNγ and IL-17) expression were
159 observed (Supplemental Figure 2A-E).

160 To investigate if OCA-B expression impacts Th1 or Th17 mediated adoptive transfer EAE,
161 CD4$^+$ T cells purified from donors were polarized in vitro into Th1 and Th17 cells as previously
162 described (43, 44). 3×10^6 Th1- or Th17-polarized CD4$^+$ cells were transferred into naïve age-
163 matched wild-type male C57BL/6 recipients by i.p. injection. EAE onset in mice receiving either
164 Th1- or Th17-polarized control cells was rapid and severe (Figure 2A-B). In contrast to the mild
165 protection observed with OCA-B deficiency in standard C57BL/6 EAE, mice adoptively transferred
166 with T cells lacking OCA-B were almost completely protected from clinical disease regardless of
167 their polarization state. Interestingly, the ability to initially polarize CD4$^+$ T cells into Th1 and Th17
168 effectors in vitro was only minimally affected by OCA-B loss (Supplemental Figure 2F-H), whereas
169 cells taken from the CNS of engrafted recipient mice at day 15 not only showed decreased CNS
170 infiltration but also reduced IL-17 expression (Figure 2C-F). This effect appeared to be specific to
171 IL-17, as no significant difference in IFNγ expression was observed (Supplemental Figure 2I).
172 These results indicate a central role for OCA-B in promoting robust neuroinflammatory T cell
173 responses upon antigen reencounter in adoptive transfer EAE models.

174 *OCA-B is dispensable for neurotropic viral clearance.* To investigate if T cell OCA-B
175 deletion impacts the ability to mount immune responses and control CNS viral infection, male
176 *Ocab*$^{fl/fl}$;CD4-Cre and *Ocab*$^{fl/fl}$ littermate controls were intracranially inoculated with 1500 plaque-
177 forming units (PFU) of the John H. Muller strain of murine hepatitis virus (JHMV), a β-coronavirus

178 adapted to infect glial cells (astrocytes, microglia and oligodendrocytes) in the mouse brain and
179 spinal cord. Inoculation with JHMV results in acute encephalomyelitis and chronic demyelination
180 similar to autoantigen-driven EAE. Disease severity was determined by evaluating clinical scores
181 over 21 days post-infection (dpi). *Ocab*$^{fl/fl}$;CD4-Cre animals showed negligible differences in
182 clinical scores compared to *Ocab*$^{fl/fl}$ littermates (Figure 3A), suggesting that OCA-B loss preserves
183 baseline T cell responses to acute infection. Spinal cords were taken on 12 and 21 dpi for
184 immunofluorescence and histological analysis to investigate differences in demyelination. MBP
185 immunofluorescence at 12 dpi showed similar demyelination and immune infiltration in both
186 Ocab$^{fl/fl}$ and Ocab$^{fl/fl}$;CD4-Cre spinal sections (Figure 3B-C). Similarly, LFB histology of brain
187 tissue at 21 dpi showed no significant differences in demyelination between OCA-B deficient and
188 control infected animals (Supplemental Figure 3A-B). Flow cytometric analysis of brain tissue
189 showed no significant differences in infiltrating CD4$^+$ T cell numbers or IFNγ expression at 7, 12,
190 or 21 dpi (Figure 3D-F, and Supplemental Figure 3C). Similarly, no differences in either total CD8$^+$
191 T cell numbers, or the percentage or numbers of IFNγ-expressing CD8$^+$ T cells was observed
192 (Supplemental Figure 3D-F). Half brain homogenates were collected on 7, 12 and 21 dpi to
193 measure viral titers and clearance. *Ocab*$^{fl/fl}$;CD4-Cre and *Ocab*$^{fl/fl}$ littermate control animals
194 showed similar titers at dpi 7 and 12, and virus was undetectable at day 21 regardless of genotype
195 (Figure 3G). This result suggests that OCA-B is dispensable for immune responses to and
196 clearance of neurotropic viruses.

197 *OCA-B expressing CD4$^+$ T cells display pathogenic stem-like properties and preferentially*
198 *transfer demyelinating disease.* We used a recently described OCA-B-mCherry reporter mouse
199 (29) to evaluate OCA-B expression within CNS infiltrating T cells. EAE was induced in female
200 C57BL/6 homozygous OCA-B-mCherry reporter mice with MOG_{35-55}, and CNS-infiltrating CD4$^+$ T
201 cells assessed by flow cytometry at peak clinical disease. mCherry-positive T cells showed
202 increased CD44 and CD62L co-expression, indicative of increased memory-like cells in the OCA-
203 B expressing population (Figure 4A). The association of OCA-B expression with a memory-like
204 profile was observed in the brain, spine and draining cervical lymph nodes (Figure 4B).
205 Interestingly, the frequency of CD44$^+$CD62L$^-$CD4$^+$ T cells was elevated within the OCA-B
206 expressing population specifically within the cervical lymph nodes (Supplemental Figure 4A).

207 Memory-like CD4$^+$ T cells have been implicated as major orchestrators of autoimmune
208 demyelination in mice and humans (9–12, 14, 15, 45). To see if this memory-like profile of OCA-
209 B expressing CD4$^+$ T cells is specific to CNS infiltrating cells, we performed flow cytometry using

210 draining lymph node and splenic T cells from MOG-primed OCA-B-mCherry reporter mice. Similar
211 to OCA-B$^+$ CNS infiltrating cells, OCA-B expressing CD4$^+$ T cells taken from the cervical lymph
212 node and spleen showed increased CD44 and CD62L co-expression (Figure 4C-D).

213 We next evaluated OCA-B-mCherry positive and negative populations by RNA
214 sequencing of CD4$^+$ T cells isolated from the lymph nodes of 14-day MOG-primed mice. ~1500
215 genes were upregulated and ~350 downregulated in OCA-B expressing compared to OCA-B
216 negative cells (Supplemental Table 1). Upregulated genes in OCA-B expressing cells included
217 *Cxcr6*, *Slamf6*, *Il23r*, *Rorc*, *Ifng*, *Bcl6*, and *Il17a* while downregulated genes included *Foxp3*, *Il7r*
218 and *Ccr9* (Figure 4E-F). Expression of *Tcf7* (which encodes TCF1) was high within both OCA-B
219 positive and negative populations (Supplemental Table 1). Gene ontology (GO) and pathway
220 analysis of upregulated genes show enrichment for terms associated with autoimmune diseases
221 including lupus, autoimmune thyroid disease, and type-1 diabetes (Figure 4G, and Supplemental
222 Table 2).

223 To determine if OCA-B expression can be used to prospectively identify viable pathogenic
224 CD4$^+$ T cell populations, we used OCA-B-mCherry reporter mice as donors in passive transfer
225 EAE. 11-week-old male and female littermates homozygous for the OCA-B-mCherry reporter
226 were primed for 14 days with MOG_{35-55} in CFA as previously described (44). CD4$^+$ T cells were
227 isolated from spleen and lymph nodes and sorted based on mCherry expression (Supplemental
228 Figure 4B). 9×10^5 mCherry negative and positive cells were cultured in Th1 polarizing conditions
229 and subsequently transferred into age-matched male C57BL/6 recipients as previously described
230 (14). Disease progression was measured by clinical score and normalized weight. Recipients of
231 OCA-B-expressing mCherry positive cells showed increased clinical disease severity and weight
232 loss compared to mCherry negative recipients (Figure 4H and Supplemental Figure 4C). These
233 findings indicate that OCA-B marks CD4$^+$ T cells with pathogenic stem-like gene expression and
234 can be used to prospectively identify peripheral CD4$^+$ T cells with elevated encephalitogenic
235 properties.

236 *OCA-B promotes neuroinflammation in relapsing-remitting EAE models via control of*
237 *stem/memory-like T cell populations.* In contrast to the chronic form of EAE that develops in
238 C57BL/6 mouse models, EAE on the NOD background exhibits a relapsing-remitting pattern that
239 more closely mimics human disease (40). To study the impact of OCA-B loss in T cells on mouse
240 models that more closely resemble human MS disease patterns, we utilized *Ocab* T cell
241 conditional knockout mice crossed to the NOD background (30). EAE was induced in 15-18 week

242 old female NOD.*Ocab*$^{fl/fl}$;CD4-Cre and littermate control NOD.*Ocab*$^{fl/fl}$ mice with MOG_{35-55}. Clinical
243 scores and weights were recorded for 47 days to observe initial disease onset, relapse and
244 relapse recovery. No significant differences in clinical scores were observed between groups at
245 disease onset (day 10-19), however following the primary remission, NOD.*Ocab*$^{fl/fl}$;CD4-Cre
246 animals were almost completely protected against disease relapse (Figure 5A). Individual NOD
247 mouse clinical scores are shown in Supplemental Figure 5A-B. Normalized weights of animals
248 also reflected the protective effect of OCA-B loss in T cells at relapse (Figure 5B).
249 To understand differences in CNS-infiltrating T cells underlying relapse protection at a
250 population and transcriptional level, we performed single-cell RNA sequencing (scRNA-seq) of
251 CD3ε^{+} T cell isolates from CNS (brain + spinal cord) at remission (day 24) and peak relapse (day
252 33). Cells from 3-6 NOD.*Ocab*$^{fl/fl}$;CD4-Cre and NOD.*Ocab*$^{fl/fl}$ littermate controls were collected and
253 combined for analysis. 7799 (remission) and 9224 (relapse) *Ocab* knockout, and 6009 (remission)
254 and 7525 (relapse) control cells were used for analysis, with an average per cell read depth
255 ranging from 90,000 to 190,000. For remission, UMAP clustering using both genotypes revealed
256 16 clusters corresponding to a broad T cell repertoire consisting of natural-killer T (NKT) cells (the
257 largest cluster) and different CD4^{+} and CD8^{+} subsets (Figure 5C). Noteworthy clusters based on
258 mRNA expression included proliferating (*Ki67*, *Pcna*, *Mcm2*), Th1-like (*Tbx21*, *Ifng*, *Tnf*, *Il12rb2*)
259 and Treg (*Foxp3*, *Ctla4*) (Supplemental Table 3). Feature plots for *Foxp3* and *Mki67* are shown
260 in Figure 5D. Additional feature plots for *Cxcr6*, *Il23r* and *Bach2* are shown in Supplemental Figure
261 5C. Notably there was a large decrease in NKT cell numbers in knockout mice (36% control vs.
262 14% experimental). Within this cluster, changes in gene expression between control and
263 conditional knockout groups were minimal. Most NKT cells from both groups showed a limited
264 inflammatory cytokine response, consistent with the lack of clinical disease at remission
265 (Supplemental Figure 5D). The decrease in the large NKT population in the experimental group
266 proportionally increases the percentage contribution of the other clusters, and therefore similar or
267 decreased percentages of these cells identifies reduced populations which correlate with
268 protection from relapse, e.g. proliferating T cells. Other clusters such as Tregs increased
269 disproportionately. Differential gene expression analysis of key clusters (Treg, Proliferating, and
270 Th1-like) revealed increased expression of *Slamf6* in Tregs lacking OCA-B, while OCA-B deficient
271 proliferating and Th1-like cells showed decreased expression of genes associated with
272 quiescence (*Btg1* and *Samhd1*), memory/stemness (*Slamf6*, *Tcf7*, and *Sell*) and pathogenicity
273 (*Tcf7* and *Tox* co-expression, Figure 5E). Spectral cytometry showed no significant difference in
274 the frequency of CNS infiltrating CD4^{+} T cells between groups at remission (Figure 5F). However,

275 OCA-B deficient CD4+ T cells did show a significant reduction in CXCR6 and IFNγ/GM-CSF co-
276 expression, indicative of reduced Th17 pathogenicity (Figure 5G-I). These results indicate that
277 loss of OCA-B in T cells selectively reduces proliferation and differentiation of pathogenic
278 stem/memory-like CD4+ T cells during disease remission.

279 At relapse, multiple CNS-infiltrating stem-like and effector CD4+ and CD8+ control T cell
280 populations were present (Figure 6A and Supplemental Figure 6A, Supplemental Table 4). TCR
281 sequencing revealed an expansion of a subset of TCR clones in the OCA-B deficient CD8 clusters
282 while most other clusters were highly polyclonal (Figure 6B). Comparing the 10 most expanded
283 TCR clonotypes between knockouts and controls, there were several clonotypes that were shared
284 but differentially expanded (Figure S6B and Supplemental Table 5). A "Ccr9 stem-like" cluster
285 expressing the gut homing chemokine receptor *Ccr9*, as well as *Ccr7*, *Bach2*, and *Tcf7* notably
286 appeared at relapse (Figure 6C and Supplemental Table 4). TCR clonotype analysis indicated
287 that this population was highly polyclonal (Figure 6B). Additionally, a "Stem-like CD4-2" cluster
288 expressing *Tcf7*, Ccr7, *Bach2, Cd44* and low-level *Cxcr6*, and a prominent "Th17-like" cluster
289 expressing *Tcf7, Cd44*, *Il1r1, Lgals3*, and higher levels of *Cxcr6* was identified (Figure 6C). This
290 latter cluster likely contains pathogenic effector cells.

291 In the absence of OCA-B, NKT cell populations were normalized compared to the
292 remission timepoint, and several clusters showed major changes in the percentage of cells
293 including most prominently the Ccr9-stem-like cells which were much more prevalent (Figure 6D).
294 Feature plots comparing OCA-B T cell deficient mice to littermate controls for *Ccr9* and the
295 transcription factors *Tcf7* and *Bach2* are shown in Figure 6D. The cells were also marked by the
296 expression of *Cd4*, *Tox, Ccr7, Ccr4* and limited expression of *Sell* (Figure 6C).

297 RNA velocity analysis of spliced and unspliced transcripts (46) identified clusters of T cells,
298 most bearing static gene expression profiles consistent with terminal differentiation, but some with
299 differentiating or transitional gene expression (Figure 6E). Notably, OCA-B knockout cells showed
300 increased transcriptional stasis within the Ccr9-stem-like and proliferating clusters, and a
301 decreased transcriptional directionality of Th17 cells towards gd17 cells, the latter of which
302 express high levels of pathogenic markers including *Il1r1*, *Cxcr6*, and *Lgals3* (Supplemental
303 Figure 6A). Pseudotime analysis identified a transcriptional capacity in the control *Ccr9*
304 expressing population to differentiate into pathogenic Th17-like cells, whereas cells lacking OCA-
305 B were limited in this capacity, possibly resulting in the accumulation of these cells (Supplemental
306 Figure 6D). These changes culminated in the Th17-like effector knockout cells expressing
307 reduced pathogenicity-associated genes such as *Pdcd1*, *Tigit* and *Il1r1* (Figure 6F). Together

308 these results suggest OCA-B mediates the transition of non-pathogenic stem-like cells to
309 pathogenic Th17 cells which ultimately drive disease relapse.

Discussion

The development of therapies that inhibit autoimmunity while minimizing impacts on normal immune function remains a critical unmet goal in the field. In this study, we show that expression of mRNA encoding the transcriptional co-regulator OCA-B is elevated in $CD4^+$ T cells from SPMS brain tissue, and that OCA-B promotes the pathogenic maturation of T cells and establishment of CNS autoimmunity, in particular episodes of relapse. Loss of OCA-B attenuates these populations in chronic EAE, in adoptive transfer EAE, and in NOD.EAE during episodes of remission. During relapse, OCA-B T cell knockout mice are almost completely protected, and accumulate a population of $CD4^+$ T cells expressing *Ccr9*, *Bach2*, and *Tcf7*. OCA-B expression also marks viable pathogenic stem/memory-like $CD4^+$ T cells that preferentially transfer EAE. Furthermore, the effects of modulating OCA-B are selective, as responses to infection with a neurotropic coronavirus that generates similar clinical symptoms but lacks an autoantigen were largely unaffected.

OCA-B is a member of a small family of transcription co-regulators that also includes OCA-T1, OCA-T2 and IκBζ (47, 48). It docks with Oct1 upon $CD4^+$ T cell activation to directly regulate immunomodulatory genes such as *Il2*, *Ifng*, *Il17a*, Tbx21 (T-bet) and *Csf2* (*Gmcsf*). Rather than functioning as a primary inducer of these genes, it is required for their robust expression upon antigen reencounter (20, 30). Notably, unlike transcription factors such as NF-AT, AP-1 and NF-κB, Oct1 and OCA-B are dispensable for normal primary T cell responses (20). These findings predict important roles for OCA-B in $CD4^+$ T cells specifically in situations of antigen reencounter, which is a necessary feature of autoimmunity. Conditional T cell knockout of Oct1 reduces EAE severity, with reduced proinflammatory cytokine expression and increased anergy (21). Deletion of Oct1 in T cells was dispensable for neurotropic viral clearance (21), however the ubiquitous expression of Oct1 in adult tissue limits its translational potential. In contrast, OCA-B expression is largely confined to B and T cells and whole-body knockout mice are viable and fertile (49). OCA-B is highly expressed in B cells and required for germinal center formation (49, 50). It is expressed in $CD4^+$ T cells upon activation at levels 50-100-fold less than in B cells (30, 51, 52). This suggests that with proper therapeutic dosing, OCA-B could be inhibited selectively in T cells with minimal impact to the B cell compartment. Short-term administration of an OCA-B peptide mimic that inhibits OCA-B's downstream effector functions reverses spontaneous type-1 diabetes in NOD mice (30). However, toxicity limits its efficacy, including within EAE models. Further research is required for the development of safe and effective OCA-B inhibitors.

342 OCA-B whole body knockout animals are partially protected from EAE (39), however, the
343 known activity of OCA-B in B cells made it unclear if the protection is T cell-derived. Here we
344 show that OCA-B promotes EAE pathogenesis through T cells. Opportunistic infections and
345 reactivation of latent CNS-tropic viruses are significant barriers for MS therapeutics that focus on
346 global immune suppression as a therapeutic mechanism. When OCA-B T cell conditional
347 knockout mice are challenged with the neurotropic coronavirus JHMV, there is little difference in
348 their ability to mount immune responses and control virus replication. These data are consistent
349 with previous findings that OCA-B loss in T cells preserves lymphocytic choriomeningitis virus
350 (LCMV) acute viral infection response, instead selectively impacting memory recall responses
351 (20, 29). This finding provides a potential therapeutic window in which targeting the low levels of
352 OCA-B in T cells could be used to blunt autoimmunity while sparing baseline immune responses.
353 Unlike the significant but modest protection observed in chronic C57BL/6 EAE, OCA-B
354 loss in adoptive transfer EAE almost completely protects recipient animals from disease. This
355 may indicate that adoptive transfer EAE models involve more autoantigen re-exposures, as
356 transferred T cells must re-encounter antigen in a naïve host before promoting disease. Protection
357 was observed regardless of whether donor cells were Th1- or Th17-polarized, indicating that
358 OCA-B functions through a mechanism that parallels rather than enforces the Th1/Th17
359 paradigm. We therefore sought other mechanisms that might explain why OCA-B T cell knockouts
360 are so strongly protected.
361 Recent findings indicate an emerging role for stem/memory-like T cells in promoting
362 autoimmunity (45, 53, 54). For example, myelin-specific $CD4^+$ T cells in MS patients show signs
363 of a previously activated, memory-like phenotype compared to healthy controls (9, 10, 12).
364 Furthermore, memory-like Th1 and Th17 cells are increased in the peripheral blood of MS patients
365 and display increased pathogenicity compared to conventional Th17 Cells (55). Similarly, in EAE
366 models, peripheral central memory-like $CD4^+CD44^{hi}CD62L^{hi}$ T cells confer increased disease
367 severity upon transfer (14). Both Oct1 and OCA-B promote the functionality of long-lived $CD4^+$
368 memory T cells following antigenic rechallenge (29, 56). An OCA-B-mCherry reporter mouse
369 allele, which effectively labels memory progenitor $CD4^+$ T cells during acute infection (29), also
370 labels $CD4^+$ T cells that preferentially confer EAE. OCA-B^{hi} cells taken from the CNS at peak EAE
371 selectively express stem/memory markers. Further profiling OCA-B^{hi} $CD4^+$ T cells suggests that
372 OCA-B promotes the transition of non-pathogenic stem-like cells to a pathogenic state associated
373 with markers such as *Cxcr6*, *Slamf6*, *Ifng*, and *Il17a*. Elevated *Pou2af1* (*Ocab*) transcripts are
374 also found in pathogenic Th17 cell populations (57). The connection between OCA-B expression

375 and pathogenic memory/stem-like T cells likely has not been appreciated before because OCA-
376 B is expressed at levels too low to be reproducibly captured with many current single-cell RNA-
377 seq technologies.

378 Relapsing-remitting EAE models have been developed using the Swiss Jim Lambert (SJL)
379 and autoimmune prone non-obese diabetic (NOD) backgrounds (40, 58). In NOD mice, MOG_{35-55}
380 EAE has been described as relapsing-remitting with minimal initial disease that increases in
381 severity upon relapse (59, 60). Using this model with the conditional *Pou2af1* allele backcrossed
382 to the NOD background (30), we found that OCA-B T cell loss minimally affects initial clinical
383 presentation, but instead protects animals specifically at relapse. The finding that OCA-B loss in
384 conventional C57BL/6 EAE results in partial protection intermediate between the initial and
385 relapse phases of NOD.EAE suggests that chronic C57BL/6 EAE may not model either initial
386 presentation or relapse accurately, but instead represents a superposition of the two.

387 Single-cell RNA expression profiling at remission identifies a significant loss of *Slamf6*,
388 *Tcf7* (encoding TCF1) and *Sell* from proliferative stem-like $CD4^+$ T cells in the OCA-B deficient
389 condition. While the majority of research on TCF1-expressing stem-like T cells focuses on $CD8^+$
390 populations with the capacity for self-renewal and differentiation into effector cells, analogous
391 descriptions have been made for $CD4^+$ populations (45, 61, 62). Indeed, autoimmune $CD4^+$ T
392 cells expressing these memory/stem-like markers have been reported as an encephalitogenic
393 reservoir that play a key role in EAE pathogenicity (45). In the same study, bulk RNA sequencing
394 associated OCA-B expression within this stem-like reservoir (45).

395 Single-cell RNA-seq at relapse identified multiple emergent populations of effector T cells
396 compared to remission. Notably, there was also an accumulation of a unique population of $CD4^+$
397 cells in OCA-B T cell deficient mice. These cells are conspicuously marked by expression not
398 only of *Ccr4*, but also of *Ccr9*, which encodes a gut-homing chemokine receptor. $CCR9^+$ memory-
399 like $CD4^+$ T cells have been linked to MS and EAE protection (63). The cells also express *Bach2*,
400 a transcription regulator which was recently associated with non-pathogenic immunomodulatory
401 Th17-polarized cells in the context of C57BL/6 EAE (64). *Bach2* expression was largely
402 concentrated in the "CCR9 stem-like" cluster, which is more numerous in the knockout condition.
403 Consistently, in bulk RNA-seq *Bach2* mRNA was upregulated in $OCA\text{-}B^-$ cells ($p<10^{-13}$), although
404 with a small (+1.74) fold change (Supplemental Table 1). Similarly, recent work associates
405 *Pou2af1* (*Ocab*) with pathogenic Th17/Th1 cells compared to the non-pathogenic *Bach2*
406 expressing cells (64). In B cells, OCA-B is known to regulate *Bach2* (65), however the interplay
407 between OCA-B and Bach2 and how this influences the pathogenic maturation of Th17 cells

408 merits additional research. Velocity and pseudotime analysis indicates that these cells are
409 normally transcriptionally inclined to progress towards an highly pathogenic Th17 population, but
410 that progression stalls in mice whose T cells lack OCA-B. Consistently, the Th17 effector
411 population in OCA-B T cell knockout mice lacks expression of key genes such as *Il1r1* and *Pdcd1*,
412 both of which are associated with pathogenicity in CNS-infiltrating Th17 cells[48,64]. The cumulative
413 alterations in these populations in OCA-B knockouts likely explains why these mice are strongly
414 protected against disease relapse. In conclusion, this study indicates a prominent role for OCA-B
415 in driving stem-like $CD4^+$ T cell populations towards a pathogenic state while playing a minimal
416 role in acute antiviral responses to a CNS infection.

417 Methods

418 *Sex as a biological variable.* The objective of this study was to determine the role of the
419 transcriptional regulator OCA-B in demyelinating disease. OCA-B T cell conditional knockout mice
420 and OCA-B reporter mice were utilized in multiple mouse demyelinating disease models to
421 evaluate the impact of T cell OCA-B expression on clinical disease manifestation and the
422 phenotypes of neuroinflammatory cells, in particular T cells. Both male and female animals were
423 used for experiments except for active EAE experiments where only female animals were used
424 as these are the better model spinal cord demyelination and inflammation.

425 *Analysis of publicly available human control and MS single nuclei RNAseq dataset.* Initial
426 evaluation of *POU2AF1* expression in T cells was conducted in the interactive web browser
427 created by the authors of the dataset available at https://malhotralab.shinyapps.io/MS_broad/
428 (41). Briefly, *POU2AF1* differential gene expression was filtered to show T cell gene expression
429 by diagnosis with a minimal threshold cutoff of 10 cells per sample. Cleaned aligned matrix files
430 were then downloaded from https://zenodo.org/records/8338963 and subsequently processed by
431 using the 10X Genomics CellRanger pipeline and further analyzed using the 10X Genomics
432 Loupe Browser 7 software. 19,906 $CD4^+$ cells were then subclustered and evaluated for
433 *POU2AF1* and *IL1R1* gene expression by diagnosis.

434 *Chronic C57BL/6 EAE.* 11-12 week-old female C57BL/6 littermate animals were used for
435 all experiments. For adoptive transfer experiments using the OCA-B-mCherry reporter allele (29),
436 11 week-old females were used for chronic EAE and 9 week-old males were used as MOG_{35-55}
437 primed adoptive transfer donors. EAE was induced on day 0 by two 100 μL s.c. injections into
438 both hind flanks of 0.5 μmol/mL MOG_{35-55} peptide (University of Utah Peptide Core) emulsified in
439 complete Freud's adjuvant (CFA), comprised of incomplete Freund's adjuvant (Cat#
440 77145;ThermoFisher) together with 4 mg/mL heat-killed *M. tuberculosis* (Cat# DF3114338; Fisher
441 Scientific). Animals were given two 400 ng i.p. injections of *B. pertussis* toxin (Cat# 181; List
442 Biological Laboratories) on days 0 and 2.

443 *Clinical Scoring.* EAE clinical scores were determined using a 0-5 scale with 0.5 scoring
444 intervals: 0.5, tip of tail is limp or tail muscle strain observed; 1, complete limp tail; 1.5, complete
445 limp tail and at least one hind limb consistently falls through wire rack when animal is dropped; 2,
446 complete limp tail and one hind leg dragging without movement beyond hip; 2.5, complete limp
447 tail and dragging of both hind limbs without movement beyond hip; 3, complete hind limb paralysis;
448 3.5, complete hind limb paralysis with flat laying hind quarters and hump in upper torso; 4,

449 complete hind limb and partial forelimb paralysis, minimal movement around cage; 4.5, complete
450 hind limb and partial forelimb paralysis, no movement around cage; 5, seizure or death. Animals
451 scoring a ≥4 for more than 48 hours were euthanized and scored 5 for the remainder of the
452 experiment. JHMV clinical disease was evaluated using previously described 0-4 point scale (67).
453 *Immunofluorescence and Histology.* Spinal columns were isolated from C57BL/6 Ocab$^{fl/fl}$
454 and Ocab$^{fl/fl}$;CD4-Cre animals after EAE or JHMV induced demyelination and fixed overnight in in
455 4% paraformaldehyde at 4C. Spinal cords were subsequently isolated and cryoprotected in 30%
456 sucrose for 3-5 days. Thoracic and lumbar sections were embedded in optimum cutting
457 temperature (OCT) compound (ThermoFisher Scientific) and frozen and stored at -80C. 8 µm
458 spinal sections were cut by cryostat and stained with Luxol fast blue (Cat# 212170250;
459 ThermoFisher) along with hematoxylin (Cat# 8495; ENG Scientific) and eosin (Cat# E511-25;
460 Fisher Chemical). Demyelination was assessed by dividing the area of demyelinated white matter
461 by total white matter as previously described (68, 69). For immunofluorescence, spinal cord
462 sections were blocked in 5% normal goat serum (NGS; Cat# 005-000-121, Jackson
463 ImmunoReseach) and 0.1% Tween-20 for 1 hour at room temperature. Sections were stained
464 overnight at 4°C with primary antibody rabbit anti-MBP (1:1000; Cat# PA1050, Boster), followed
465 by secondary antibody goat anti-rabbit conjugated with Alexa Fluor 488 (1:750; Cat# A11008,
466 Invitrogen) for 2 hours at room temperature. Primary and secondary antibodies were diluted in
467 1% bovine serum albumin (BSA) and 0.1% Tween-20. Slides were cover-slipped using
468 Fluoromount-G with DAPI (Cat# 00495952, Invitrogen). Sections were imaged with a Zeiss
469 Axioscan 7 Microscope Slide Scanner using a 20× objective.
470 *Flow cytometry and spectral cytometry.* Spinal cords and brains were harvested at peak
471 disease or specified timepoint and mechanically dissociated by passing through a 100 µm cell
472 strainer. A 30/70% Percoll gradient (Cat# 17544501; Cytiva) was used to enrich mononuclear
473 cells. Cells from collected spleens and lymph nodes (cervical, brachial, axillary and inguinal) were
474 passed through a 70 µm strainer and erythrocytes lysed by ammonium-chloride-potassium lysis
475 buffer (150 mM NH_4Cl, 10 mM $KHCO_3$, 0.1 mM Na_2EDTA). For intracellular staining, cells were
476 cultured in complete media (RPMI 1640, 10% FBS, 1% Pen/Strep, Glutamax) supplemented with
477 1 µL/mL brefeldin A (Cat# 555029; Golgiplug, BD), 50 ng/mL phorbol myristate acetate (Cat#
478 P1585; Sigma-Aldrich) and 1 µg/mL ionomycin (Cat# I0634; Sigma-Aldrich) for 4 hr. Cultured
479 cells were fixed using cytofix/cytoperm (Cat# 554714; BD) according to manufacturer's protocol
480 and stained for intracellular cytokines in perm/wash buffer. Flow cytometry samples were profiled

481 using a BD Fortessa (BD Biosciences, Figure 2, 3, 4) or an Aurora spectral flow cytometer (Cytek,
482 Fig 1 and 5). FlowJo software (BD Biosciences) was used for data analysis.
483 *Pre-polarization profiling and mixed adoptive transfer.* 10 week-old C57BL/6 *Ocab*$^{fl/fl}$ and
484 *Ocab*$^{fl/fl}$*;CD4-Cre* littermates were immunized with MOG_{35-55} in CFA as described above. After 14
485 days, spleen and lymph node (cervical, axillary, brachial and inguinal) cells were isolated and
486 cultured in complete media (RPMI 1640, 10% FBS, 1% Pen/Strep, Glutamax) supplemented with
487 1 µL/mL brefeldin A (Cat# 555029; Golgiplug, BD), 50 ng/mL phorbol myristate acetate (Cat#
488 P1585; Sigma-Aldrich) and 1 µg/mL ionomycin (Cat# I0634; Sigma-Aldrich) for 4 hr. Cells were
489 stained for surface markers, fixed using the Foxp3/Transcription Factor Staining Buffer Kit
490 (Cat#00-5523-00, ThermoFisher), and stained for intracellular markers (IFNγ and IL-17).
491 *Th1 and Th17 polarization and adoptive transfer C57BL/6 EAE.* 10-12 week-old female
492 C57BL/6 littermate animals were used for all experiments. Donor animals were immunized with
493 MOG_{35-55} in CFA as above. 10-14 days post-immunization, spleen and lymph node (cervical,
494 axillary, brachial and inguinal) cells were collected and placed into mixed culture with MOG
495 peptide and cytokines at 5.0×10^6 cells/mL. For Th1 conditions, complete media was
496 supplemented with 50 μg/mL MOG_{35-55}, 6 ng/mL rmIL-6 (Cat# 216-16; Peprotech) and 2 ng/mL
497 rmIFNγ (Cat# 315-05; Peprotech). For Th17 conditions, complete media was supplemented with
498 50 μg/mL MOG_{35-55}, 8 ng/mL rmIL-23 (Cat# 1887-ML-010; R&D Systems), 10 ng/mL rmIL-1α
499 (Cat# 211-11A; Peprotech), and 10 μg/mL anti-IFNγ (Cat# BE0055; BioXcell XMG1.2). After 4
500 days of respective culture, $CD4^+$ T cells were purified using negative magnetic selection and
501 resuspended in PBS at 1.5×10^6 cells/mL. 100 μL cell suspension was injected i.p. into age-
502 matched male C57BL/6 recipients (~13 week-old at time of disease induction). Clinical disease
503 was scored for 15 days.
504 *JHMV. Ocab*$^{fl/fl}$ and *Ocab*$^{fl/fl}$;CD4-Cre C57BL/6 mice were anesthetized using isoflurane.
505 Mice were intracranially (i.c) injected with 1500 plaque-forming units (PFU) of JHMV (strain V34)
506 suspended in 30 µL Hank's balanced salt solution (ThermoFisher). Clinical disease was assessed
507 for 21 days using a previously described scale (67). Mice were sacrificed at days 7, 12, and 21
508 post-infection to assess viral titers within brain homogenates using a plaque assay previously
509 described (70). Spinal cords were taken on day 12 and 21 post-infection to assess demyelination
510 by DAPI/MBP and luxol fast blue and hematoxylin/eosin histology respectively.
511 *OCA-B-mCherry adoptive transfer EAE.* OCA-B-mCherry reporter allele animals (29) were
512 primed for 14 days with MOG_{35-55} in CFA as described above. After priming, spleen and lymph

513 nodes were collected and $CD4^+$ T cells were purified by magnetic negative selection (Miltenyi Bio
514 kit and LS columns). Non-$CD4^+$ T cells were removed from the LS column and placed on ice for
515 subsequent in vitro culture. Purified $CD4^+$ T cells were separated by OCA-B-mCherry expression
516 (PE-Texas Red) using flow automated cell sorting (FACS). OCA-B-mCherry positive and negative
517 $CD4^+$ T cells were placed into mixed culture in complete medium with the previously purified non-
518 $CD4^+$ T cells at a 1:10 ratio ($CD4^+$ to non-$CD4^+$) at 1.0×10^6 cells/mL. The culture was
519 supplemented with 20 μg/mL MOG_{35-55} and 0.5 ng/mL IL-12p70 (Cat# 210-12; Peprotech). After
520 two days of culture, $CD4^+$ T cells were again purified through negative magnetic selection. Purified
521 $CD4^+$ T cells from OCA-B-mCherry positive and negative cultures were resuspended in PBS at
522 8.8×10^6 cells/mL. 100 μL cell suspension was injected i.p. into age-matched male C57BL/6
523 recipients. Clinical disease was assessed for 24 days.

524 *Bulk RNA-seq.* OCA-B-mCherry reporter mice (n=9) were primed for 14 days with MOG_{35-}
525 $_{55}$ in CFA as described above. After priming, lymph nodes (cervical, axillary, brachial and inguinal)
526 were isolated and mCherry positive and negative $CD4^+$ T cells were collected by FACS. Total
527 RNA, three groups (pooled 3 mice each), was isolated using the Quick RNA micro kit (Cat#
528 R1050; Zymo Research) with DNase treatment (Cat# 79254; Qiagen). RNA concentration was
529 measured with a Qubit RNA HS Assay Kit (Cat# #Q32855; Fisher Scientific). RNA quality was
530 evaluated with an RNA ScreenTape Assay (Cat# 5067-5579, 5067-5580; Agilent Technologies).
531 Total RNA samples (5-500 ng) were hybridized with NEBNext rRNA Depletion Kit v2 (Cat# E7400;
532 New England Biolabs) to diminish rRNA from the samples. Stranded RNA sequencing libraries
533 were prepared as described using the NEBNext Ultra II Directional RNA Library Prep Kit for
534 Illumina (Cat# E7760L; New England Biolabs). Purified libraries were qualified on an 4150
535 TapeStation (Agilent Technologies) using a D1000 ScreenTape assay (Cat# 5567-5582, 5067-
536 5583; Agilent Technologies). The molarity of adapter-modified molecules was defined by
537 quantitative PCR using the Kapa Biosystems Kapa Library Quant Kit (Cat# KK4824Roche).
538 Individual libraries were normalized to 5 nM. NovaSeq 150×150 bp sequencing libraries were
539 chemically denatured and applied to an Illumina NovaSeq flow cell using the XP workflow
540 (20043131). Following transfer to an Illumina NovaSeq 6000 instrument, 150×150 cycle paired-
541 end sequencing was performed using a S4 reagent Kit v1.5 (Cat# 20028312; Illumina). 8-11
542 million reads were generated per sample and were aligned to the *GRCm38* mouse reference
543 genome. Differential gene expression and pathway analysis were conducted using the DESeq2
544 and Enrichr R packages.

545 *NOD-EAE.* 15-18 week-old female littermate *Ocab*$^{fl/fl}$ and *Ocab*$^{fl/fl}$;CD4-Cre animals
546 backcrossed to a NOD strain background (30) were used for all experiments. EAE was induced
547 by two 100 μL s.c. injections into both hind flanks of 0.5 μmol/mL MOG_{35-55} peptide emulsified in
548 incomplete Freuds adjuvant (Cat# 77145; ThermoFisher) supplemented with 4 mg/mL heat-killed
549 *M. tuberculosis* (Cat# DF3114338; Fisher Scientific) to form CFA. Animals were given two 400 ng
550 i.p. injections of *Bordetella pertussis* toxin (Cat# 181; List Biological Laboratories) on days 0 and
551 2. Clinical disease was assessed over 47 days using a 5-point scale described below. Remission
552 timepoints were determined to be between days 22-26 while relapse was determined to be
553 between days 26-39.
554 *Single-cell RNA-seq.* NOD.*Ocab*$^{fl/fl}$ and NOD.*Ocab*$^{fl/fl}$;CD4-Cre animals were induced with
555 EAE and monitored for disease progression. Brains and spinal cords were isolated on day 24
556 (remission) and day 33 (relapse), and processed for FACS sorting. Viable cells were sorted by
557 CD3ε using a FACSAria (BD Bioscience). Cells from each condition were isolated from 3-4 mice
558 and combined. Cells were processed using the 5' 10X Genomics Chromium platform according
559 to the manufacturer's instructions. Paired-end high-throughput sequencing (125 cycles) was
560 performed using a NovaSeq instrument (Illumina). Sequencing reads were processed by using
561 the 10X Genomics CellRanger pipeline and further analyzed using the Seurat R package.
562 Analysis of cells used a standard filtering protocol removing cells with unique feature counts of
563 >5,000 or <100, as well as cells with >10% mitochondrial counts (indicative of dead cells). No
564 more than 10% of total cells were removed by this process. Cells were subjected to unsupervised
565 hierarchical clustering followed by uniform manifold approximation and projection (UMAP) to
566 visualize clusters with similar gene expression and their relative positions. RNA velocity analysis
567 was performed using velocyto.R version 0.6 to model cell state transitions using the guidelines
568 provided in Manno et al. (46) and the associated repository at https://github.com/velocyto-
569 team/velocyto.R. High dimensional velocity vectors were graphed on the predefined Seurat
570 UMAP projection using localized average grid projections. Pseudotime analysis was conducted
571 using Seurat and Monocle3 packages. Integrated data was divided into subset based on genotype
572 and Monocle3 was used to calculate trajectory, order cells and plot pseudotime for each condition.
573 *Statistics.* Multiple two-tailed student's t-tests were used to determine statistical
574 differences in EAE clinical scores and all error bars denote ±SEM unless otherwise noted. Two-
575 way ANOVA was used to determine differences in weight loss throughout disease progression.
576 GraphPad Prism software was used for all statistics and graphing. Two-tailed student's t-tests

577 were used to determine statistical differences in cell populations observed by flow cytometry and
578 all error bars represent ±SD unless otherwise noted. For all figures, ns = $p>0.05$, * = $p\leq0.05$, ** =
579 $p\leq0.01$, *** = $p\leq0.001$, **** = $p\leq0.0001$.

580 *Study approval.* All animal experiments were performed in strict accordance with the NIH
581 guide for the Care and Use of Laboratory animals and institutional guidelines for animal care at
582 the University of Utah under approved protocol #00001553.

583 *Data availability.* All RNA sequencing, single-cell sequencing, and single-cell T cell V(D)J
584 sequencing data associated with the findings of this study have been deposited to NCBI's GEO
585 database under accession code GSE243727.

586 Figure legends

587 **Figure 1. OCA-B loss protects animals from chronic EAE.** (**A**) CD4$^+$ T cell nuclei from single-
588 nucleus RNAseq data of primary-progressive (PPMS), relapsing-remitting MS (RRMS), and
589 secondary-progressive MS (SPMS) patient lesions and controls (41) were identified and tested in
590 silico for *POU2AF1* expression, which is displayed as counts per million. (**B**) The CD4$^+$ T cell
591 nuclei were reclustered and displayed as UMAP feature plots showing *POU2AF1* (left) and *Il1R1*
592 (right) expression in CTR and SPMS brain tissue. Red arrow highlights a likely pathogenic CD4$^+$
593 population expressing high levels of *IL1R1*. (**C**) *Ocab*$^{fl/fl}$ (n=16) and *Ocab*$^{fl/fl}$;CD4-Cre (n=22) mice
594 were injected with MOG$_{35-55}$ peptide in CFA and *pertussis* toxin to induce EAE. Clinical scores
595 were evaluated after EAE induction to determine disease progression. (**D**) Animal weights were
596 recorded to evaluate weight loss as a measurement of disease progression. (**E**) Representative
597 DAPI/MBP immunostaining of thoracic sections taken from mice 15 days after EAE induction.
598 Areas of demyelination are marked by decreased MBP staining (green) and often coincide with
599 increased cellular infiltration (blue). (**F**) Quantification of demyelination in *Ocab*$^{fl/fl}$ (n=5) and
600 *Ocab*$^{fl/fl}$;CD4-Cre mice (n=6). (**G**) Brain and spinal cords were isolated on day 15 of EAE and
601 analyzed by spectral cytometry. Representative flow cytometry plots of CD45$^+$TCRβ$^+$ CNS
602 infiltrating T cells showing frequency of CD4$^+$ and CD8$^+$ T cells. (**H**) Quantification of the number
603 of CNS infiltrating CD4$^+$ T cells. *Ocab*$^{fl/fl}$ (n=9) and *Ocab*$^{fl/fl}$;CD4-Cre (n=13). (**I**) Representative
604 plots showing frequency of MOG$_{38-49}$ tetramer-positive CD4$^+$ T cells. (**J**) Quantification of the
605 frequency and count of MOG$_{38-49}$ tetramer-positive CD4$^+$ T cells. *Ocab*$^{fl/fl}$ (n=9) and *Ocab*$^{fl/fl}$;CD4-
606 Cre (n=13). For clinical scores and normalized weights, values represent mean ±SEM. All other
607 values represent mean ±SD.

608

609 **Figure 2. OCA-B promotes Th1 and Th17 adoptive transfer EAE through recall response.**
610 (**A,B**) *Ocab*$^{fl/fl}$ and *Ocab*$^{fl/fl}$;CD4-Cre mice were primed with MOG$_{35-55}$ peptide in CFA for 10-14
611 days. Cells from the spleens and lymph nodes of primed mice were isolated and cultured for 4
612 days in Th1 or Th17 polarizing conditions. 3.0x10^6 Th1- or Th17-polarized cells were injected i.p.
613 into C57BL/6 wildtype recipient mice (Th1: *Ocab*$^{fl/fl}$ n=5, *Ocab*$^{fl/fl}$;CD4-Cre n=5) (Th17: *Ocab*$^{fl/fl}$
614 n=3, *Ocab*$^{fl/fl}$;CD4-Cre n=4). Clinical scores were assessed for 14-15 days. (**C**) At Th17 adoptive
615 transfer EAE endpoint, brains and spinal cords were analyzed by flow cytometry. Quantification
616 of brain- and spinal cord-infiltrating CD4$^+$ T cells following Th17 adoptive transfer. (**D**)
617 Representative flow cytometry plots showing the frequency of IFNγ and IL-17 expressing CD4$^+$ T

618 cells within the spines of Th17 recipient mice. (**E**) Quantification of IL-17 frequency in spinal cord
619 infiltrating CD4$^+$ T cells. (**F**) Quantification of the total count of IL-17$^+$ CD4$^+$ T cells within the spinal
620 cord of recipient mice. For clinical scores, values represent mean ±SEM. All other values
621 represent mean ±SD.
622
623
624 **Figure 3. OCA-B is dispensable for T cell response to CNS infection with a neurotropic**
625 **virus.** (**A**) *Ocab*$^{fl/fl}$ (n=19) and *Ocab*$^{fl/fl}$;CD4-Cre (n=17) mice were injected intracranially with 1500
626 PFU JHMV. Clinical scores were recorded for 21 days post infection (dpi). (**B**) Representative
627 DAPI/MBP immunofluorescence staining of spinal cord sections at 12 dpi. Demyelinated areas
628 are marked by decreased MBP staining (green) and often coincide with increased cellular
629 infiltration (blue). (**C**) Quantification of % demyelination in spinal cord sections. (n=7 per group).
630 Half brains were taken at 7, 12, and 21 dpi for flow cytometric and viral titer analysis. (**D**)
631 Quantification of CD4$^+$ T cell counts within half brain at 7, 12, 21 dpi. *Ocab*$^{fl/fl}$ (n=7-9 per time
632 point) and *Ocab*$^{fl/fl}$;CD4-Cre (n=6-7 per time point). (**E**) Representative plots showing the
633 frequency of IFNγ expressing CD4$^+$ T cells 7, 12, and 21 dpi. (**F**) Quantification of frequency of
634 IFNγ expressing CD4$^+$ T cells. *Ocab*$^{fl/fl}$ (n=7-9 per time point) and *Ocab*$^{fl/fl}$;CD4-Cre (n=6-7 per
635 time point). (**G**) Viral titers of half-brains at dpi 7, 12, and 21 (n.d., not detected). *Ocab*$^{fl/fl}$ (n=7-9
636 per time point) and *Ocab*$^{fl/fl}$;CD4-Cre (n=6-7 per time point). These data represent the combined
637 results of two independent experiments. For clinical scores, values represent mean ±SEM. All
638 other values represent mean ±SD.
639
640 **Figure 4. OCA-B expression marks encephalitogenic stem-like CD4$^+$ T cells.** (**A**) OCA-B-
641 mCherry mice were injected with MOG$_{35-55}$ peptide in CFA and *pertussis* toxin to induce EAE.
642 Cervical lymph nodes (CLNs), brains, and spines were isolated at peak disease (day 15) and
643 analyzed by flow cytometry for mCherry, CD44 and CD62L expression. (**B**) CD44$^+$ and CD62L$^+$
644 expressing CD4$^+$ T cells were quantified based on mCherry expression. Mean values are shown
645 from n=5 biological replicates. (**C**) OCA-B-mCherry mice were injected with MOG$_{35-55}$ peptide in
646 CFA, and after 14 days CD4$^+$ T cells within CLNs and spleens were profiled by flow cytometry for
647 mCherry, CD44, and CD62L expression. (**D**) Quantification of CD44 and CD62L expression of
648 OCA-B negative and positive CD4$^+$ T cells from MOG-primed OCA-B-mCherry mice. n=3
649 biological replicates are shown. (**E**) Heatmap showing relative expression of the top 40

650 differentially expressed genes from OCA-B positive and negative CD4$^+$ T cells from bulk RNA
651 sequencing of OCA-B positive and negative CD4$^+$ T cells from MOG$_{35-55}$ primed OCA-B-mCherry
652 reporter mice. (F) Volcano plot of differentially expressed genes between OCA-B positive and
653 negative T cells (*p*-value < 0.05 and Log2 fold change > 1 are colored). (**G**) Gene Ontology (GO)
654 terms associated with OCA-B positive and negative groups. (**H**) EAE clinical scores of C57BL/6
655 wild-type mice following passive transfer of OCA-B-positive or -negative Th1 polarized CD4$^+$ T
656 cells. Clinical score values represent mean ±SEM. All other values represent mean ±SD.
657
658 **Figure 5. OCA-B promotes relapsing-remitting EAE through stem-like CD4$^+$ T cells.** (**A**)
659 NOD.*Ocab*$^{fl/fl}$ (n=19) and NOD.*Ocab*$^{fl/fl}$;CD4-Cre (n=15) mice were injected with MOG$_{35-55}$ peptide
660 in CFA and *pertussis* toxin to induce EAE. Clinical scores of animals representing relapsing-
661 remitting disease progression are shown as a function of time. (**B**) Animal weights were recorded
662 to determine weight loss throughout initial disease and relapse. (**C**) Singe cell RNA sequencing
663 was performed on pooled CD3ε$^+$ cells isolated from the brain and spine of NOD.*Ocab*$^{fl/fl}$ (n=3) and
664 NOD.*Ocab*$^{fl/fl}$;CD4-Cre (n=4) 24 days after EAE induction (remission timepoint). Cell populations
665 were plotted in a UMAP using the Seurat R package and percentages are shown for each cluster.
666 Clusters were identified through differential gene expression analysis. (**D**) Feature plots
667 comparing the expression of *Foxp3* and *Mki67* amongst clusters. (**E**) Violin plots showing the
668 expression of *Btg1*, *Samhd1*, *Slamf6*, *Tcf7, Sell* and *Tox* within the Treg, proliferating, and Th1-
669 like clusters. (**F**) CNS cells isolated at remission timepoint (day 24) were analyzed by spectral
670 cytometry. Representative flow cytometry plots and quantification showing the frequency of CD4$^+$
671 T cells between control and experimental groups. (**G**) Representative flow cytometry plots and
672 quantification showing the frequency of CXCR6 expressing CD4$^+$ T cells. (**H**) Representative flow
673 cytometry plots showing the frequency of CD4$^+$ T cells expressing IFNγ and GM-CSF. (**I**)
674 Quantification of CD4$^+$ T cells expressing IFNγ and GM-CSF. For clinical scores, data represent
675 mean ±SEM. All other data represents mean ±SD.
676
677 **Figure 6. OCA-B promotes disease relapse through control of pathogenic stem-like Th17**
678 **differentiation.** (**A**) Singe cell RNA and TCR sequencing were performed on pooled CD3ε$^+$ cells
679 isolated from the brain and spine of NOD.*Ocab*$^{fl/fl}$ (n=5) and NOD.*Ocab*$^{fl/fl}$;CD4-Cre (n=6) 33 days
680 after EAE induction (relapse timepoint). Cell populations were plotted in a UMAP using the Seurat
681 R package and percentages are shown for each cluster. Clusters were identified through

682 differential gene expression analysis. (**B**) UMAP TCR clonotype expansion between *Ocab*$^{fl/fl}$ and
683 *Ocab*$^{fl/fl}$;CD4-Cre amongst clusters. (**C**) Violin plots showing expression of *Ccr9*, *Bach2*, *Ccr7*,
684 *Tcf7*, *Cd44*, *Cxcr6*, *Il1r1* and *Lgals3* in the Ccr9 Stem-like CD4, Stem-like CD4-2, and Th17-like
685 clusters. (**D**) Feature plots comparing the expression of *Ccr9*, *Tcf7*, and *Bach2* amongst clusters**.**
686 (**E**) UMAPs showing RNA velocity of spliced and unspliced transcripts by experimental condition.
687 (**F**) Violin plots showing expression of *Pdcd1*, *Tigit*, and *Il1r1* in the Th17-like cluster between
688 control and experimental groups.

689 Supplemental figure legends

690 **Supplemental Figure 1. Minimal differences in cytokine expressing CD4$^+$ T cell, CD8$^+$ T cell,**
691 **B cell, macrophage or microglial cell counts at peak chronic EAE in OCA-B knockouts.** (**A**)
692 Representative spinal cord LFB/H&E staining of thoracic sections taken from mice 15 days after
693 EAE induction. Areas of demyelination are outlined in black and marked by increased loss of LFB
694 (blue) staining and visibility of H&E (pink) within the white matter. (**B**) Quantification of the %
695 demyelination from LFB/H&E histology. (**C**) Quantification of the frequency of CNS infiltrating
696 CD4$^+$ T cells between Ocab$^{fl/fl}$ and Ocab$^{fl/fl}$;CD4-Cre mice. (**D**) Quantification of frequency and
697 count of CD8α positive T cells between Ocab$^{fl/fl}$ and Ocab$^{fl/fl}$;CD4-Cre mice. (**E**) Quantification of
698 the number of B cells, macrophages and microglia. (**F**) Representative flow cytometry plots
699 comparing the expression of CD44$^+$ within CNS infiltrating CD8$^+$ T cells from Ocab$^{fl/fl}$ and
700 Ocab$^{fl/fl}$;CD4-Cre mice. (**G**) Quantification of the frequency of CNS infiltrating CD44$^+$ CD8$^+$ T cells
701 within Ocab$^{fl/fl}$ and Ocab$^{fl/fl}$;CD4-Cre mice. (**H**) Quantification of frequency and count of IFNγ, IL-
702 17, GM-CSF, and CD44 expressing CD4$^+$ T cells from Ocab$^{fl/fl}$ and Ocab$^{fl/fl}$;CD4-Cre mice. All data
703 represent mean $\pm$SD.
704

705 **Supplemental Figure 2. Loss of OCA-B does not strongly alter initial Th1 or Th17**
706 **polarization in vitro.** (**A**) Experimental schematic for assessing CD4$^+$ T cell differences between
707 Ocab$^{fl/fl}$ and Ocab$^{fl/fl}$CD4-Cre prior to *in vitro* Th1 or Th17 polarization. Lymph nodes (cervical,
708 brachial, axillary, and inguinal) were harvested from Ocab$^{fl/fl}$ (n=4) and Ocab$^{fl/fl}$;CD4-Cre (n=4)
709 mice following 14 days of MOG$_{35-55}$/CFA priming and analyzed by flow cytometry. (**B**) Frequency
710 of viable cells isolated from Ocab$^{fl/fl}$ and Ocab$^{fl/fl}$;CD4-Cre mice. (**C**) Total CD4$^+$ T cell numbers
711 isolated from Ocab$^{fl/fl}$ and Ocab$^{fl/fl}$;CD4-Cre mice. (**D**) Quantification of the frequency of IFNγ
712 expressing CD4$^+$ T cells isolated from Ocab$^{fl/fl}$ and Ocab$^{fl/fl}$;CD4-Cre mice. (**E**) Quantification of
713 the frequency of IL-17 expressing CD4$^+$ T cells derived from Ocab$^{fl/fl}$ and Ocab$^{fl/fl}$;CD4-Cre mice.
714 (**F**) Representative flow cytometry plots showing IFNγ and IL-17 expressing CD4$^+$ T cells from
715 Ocab$^{fl/fl}$ (n=5) and Ocab$^{fl/fl}$;CD4-Cre (n=5) mice after Th1 and Th17 *in vitro* polarization. (**G**)
716 Quantification of IFNγ expressing CD4$^+$ T cells after Th1 polarization. (**H**) Quantification of IL-17
717 expressing CD4$^+$ T cells after Th17 polarization. (**I**) Quantification of the frequency of IFNγ
718 expressing CD4$^+$ T cells isolated from the spinal cords of Th17 adoptive transfer EAE recipient
719 mice. All data represent mean $\pm$SD.
720

721 **Supplemental Figure 3. Normal immune responses to intracranial JHMV infection in the**
722 **absence of OCA-B.** (**A**) Representative LFB/H&E histology of spinal cord sections at dpi 21. (**B**)
723 Demyelination quantification of LFB/H&E histology at dpi 21. (**C**) Quantification of the number of
724 IFNγ expressing $CD4^+$ T cells at dpi 7, 12 and 21. (**D**) Quantification of the number of $CD8^+$ T cells
725 at dpi 7, 12 and 21. (**E**) Quantification of the frequency of IFNγ expressing $CD8^+$ T cells at dpi 7,
726 12 and 21. (**F**) Quantification of the number of IFNγ expressing $CD8^+$ T cells at dpi 7, 12 and 21.
727 All data represent mean ±SD.
728
729 **Supplemental Figure 4. Sorting OCA-B-mCherry reporter T cells and additional analysis of**
730 **the effects of transferring OCA-B^{hi} versus OCA-B^{lo} $CD4^+$ cells.** (**A**) Quantification of the
731 frequency of $CD44^+$ $CD62^-$ $CD4^+$ T cells within the cervical lymph nodes of OCA-B-mCherry
732 reporter mice at peak EAE by OCA-B-mCherry expression. (**B**) Gating strategy for sorting of OCA-
733 B^+ and OCA-B^- $CD4^+$ T cells. (**C**) Normalized weights of NOD.$Ocab^{fl/fl}$ and NOD.$Ocab^{fl/fl}$;CD4-Cre
734 mice following EAE induction. Normalized weight is represented by mean ±SEM. All other data
735 represent mean ±SD.
736
737 **Supplemental Figure 5. Individual NOD mouse EAE clinical scores, additional remission**
738 **scRNA-seq cluster annotation genes, and heat map of gene enrichments by cluster.** (**A**)
739 Clinical scores of individual NOD.$Ocab^{fl/fl}$ mice following EAE induction. (**B**) Clinical scores of
740 individual NOD.$Ocab^{fl/fl}$;CD4-Cre mice following EAE induction. (**C**) UMAP feature plots showing
741 expression of *Cxcr6*, *Il23r*, and *Bach2* amongst clusters at remission timepoint. (**D**) Heatmap
742 showing the top 10 genes expressed by cluster at remission EAE timepoint.
743
744 **Supplemental Figure 6. Heat map of NOD.EAE relapse gene enrichments by cluster, TCR**
745 **clonotype overlap between condition, example relapse feature plots, and pseudotime**
746 **analysis of relapse single cell RNA seq.** (**A**) Heatmap showing the top 10 genes expressed by
747 cluster at relapse EAE timepoint. (**B**) Alluvial plot showing top 10 TCR clonotype gene overlap
748 between $Ocab^{fl/fl}$ and $Ocab^{fl/fl}$;CD4-Cre groups. (**C**) UMAP feature showing the expression of *CD4*,
749 *CD8a, Tox*, *Sell*, *Ccr7*, and *Ccr4* amongst clusters at relapse timepoint. (**D**) Pseudotime analysis
750 of relapse single cell from root starting node at or near the *Ccr9*-expressing stem-like cluster.

751 Acknowledgements
752 We thank R.M. O'Connell and M. Bettini for critical reading of the manuscript. We thank J. Marvin
753 and University of Utah Health Sciences Center Flow Cytometry core, and B. Dalley, O. Allen and
754 the High-Throughput Genomics core. Peptides were synthesized by the DNA/Peptide facility. We
755 thank T. Lane for assistance with JHMV constructs, protocols and reagents. This work was
756 supported by grants from the National Institutes of Health/ National Institute of Allergy and
757 Infectious Diseases (R01AI162929 and R01AI100873) and the Praespero Foundation (Canada)
758 to DT, and training grants from the National Institute of Neurological Disorders and Stroke
759 (T32NS115664) to EPH and National Institute of Allergy and Infectious Diseases (T32AI055434)
760 to ARS.
761
762 Author contributions: E.P.H. and D.T. conceived the study. E.P.H. and A.S. performed
763 experiments. E.P.H, A.S., E.M.M. and B.T.S. analyzed data. T.E.L., B.T.S. and D.T. provided
764 critical resources and supervision for the study. E.P.H. and D.T. wrote, reviewed and revised the
765 manuscript.
766
767 Conflict of interest
768 The authors declare that they have no conflicts of interest.

769 **References**

770 1. Walton C, et al. Rising prevalence of multiple sclerosis worldwide: Insights from the Atlas of
771 MS, third edition. *Mult Scler J*. 2020;26(14):1816–1821.
772 2. Wtccc CC, et al. Genetic risk and a primary role for cell-mediated immune mechanisms in
773 multiple sclerosis. *Nature*. 2011;476(7359):214–219.
774 3. IMSGC. A high-density screen for linkage in multiple sclerosis. *Am J Hum Genet*.
775 2005;77(3):454–467.
776 4. Adorini L, Guery J-C, Trembleau S. Manipulation of the Th1/Th2 Cell Balance: An Approach
777 to Treat Human Autoimmune Diseases? *Autoimmunity*. 1996;23(1):53–68.
778 5. Langrish CL, et al. IL-23 drives a pathogenic T cell population that induces autoimmune
779 inflammation. *J Exp Med*. 2005;201(2):233–240.
780 6. Brucklacher-Waldert V, et al. Phenotypical and functional characterization of T helper 17 cells
781 in multiple sclerosis. *Brain*. 2009;132(12):3329–3341.
782 7. Montes M, et al. Oligoclonal myelin-reactive T-cell infiltrates derived from multiple sclerosis
783 lesions are enriched in Th17 cells. *Clin Immunol*. 2009;130(2):133–144.
784 8. Hartmann FJ, et al. Multiple sclerosis-associated IL2RA polymorphism controls GM-CSF
785 production in human TH cells. *Nat Commun*. 2014;5(1):5056.
786 9. Scholz C, et al. Expansion of Autoreactive T Cells in Multiple Sclerosis Is Independent of
787 Exogenous B7 Costimulation. *J Immunol*. 1998;160(3):1532–1538.
788 10. Burns JB, Bartholomew BD, Lobo ST. Isolation of CD45RO+, Memory T Cells Recognizing
789 Proteolipid Protein from Neurologically Normal Subjects. *Cell Immunol*. 2001;212(1):44–50.
790 11. Pelfrey CM, et al. Quantification of Self-Recognition in Multiple Sclerosis by Single-Cell
791 Analysis of Cytokine Production. *J Immunol*. 2000;165(3):1641–1651.
792 12. Lovett-Racke AE, et al. Decreased dependence of myelin basic protein-reactive T cells on
793 CD28-mediated costimulation in multiple sclerosis patients. A marker of activated/memory T
794 cells. *J Clin Invest*. 1998;101(4):725–730.
795 13. Lee H-G, et al. Pathogenic function of bystander-activated memory-like CD4+ T cells in
796 autoimmune encephalomyelitis. *Nat Commun*. 2019;10(1):709.
797 14. Williams JL, et al. Memory cells specific for myelin oligodendrocyte glycoprotein (MOG)
798 govern the transfer of experimental autoimmune encephalomyelitis. *J Neuroimmunol*.
799 2011;234(1–2):84–92.
800 15. Elyaman W, et al. Distinct Functions of Autoreactive Memory and Effector CD4+ T Cells in
801 Experimental Autoimmune Encephalomyelitis. *Am J Pathol*. 2008;173(2):411–422.

802 16. Maurano MT, et al. Systematic Localization of Common Disease-Associated Variation in
803 Regulatory DNA. *Science (80-)*. 2012;337(6099):1190–1195.
804 17. Graham DSC, et al. Evidence for unique association signals in SLE at the CD28–CTLA4–
805 ICOS locus in a family-based study. *Hum Mol Genet*. 2006;15(21):3195–3205.
806 18. van Heel DA. Inflammatory bowel disease is associated with a TNF polymorphism that
807 affects an interaction between the OCT1 and NF-kappaB transcription factors. *Hum Mol Genet*.
808 2002;11(11):1281–1289.
809 19. Farh KK, et al. Genetic and epigenetic fine mapping of causal autoimmune disease variants.
810 *Nature*. 2015;518(7539):337–343.
811 20. Shakya A, et al. Oct1 and OCA-B are selectively required for CD4 memory T cell function. *J*
812 *Exp Med*. 2015;212(12):2115–2131.
813 21. Kim H, et al. T cell-selective deletion of Oct1 protects animals from autoimmune
814 neuroinflammation while maintaining neurotropic pathogen response. *J Neuroinflammation*.
815 2019;16(1):133.
816 22. Vázquez-Arreguín K, et al. Oct1/Pou2f1 is selectively required for colon regeneration and
817 regulates colon malignancy. *PLOS Genet*. 2019;15(5):e1007687.
818 23. Perovanovic J, et al. Oct1 cooperates with the Smad family of transcription factors to
819 promote mesodermal lineage specification. *Sci Signal*. 2023;16(781).
820 https://doi.org/10.1126/scisignal.add5750.
821 24. Sebastiano V, et al. Oct1 regulates trophoblast development during early mouse
822 embryogenesis. *Development*. 2010;137(21):3551–3560.
823 25. Hwang SS, et al. Role of OCT-1 and partner proteins in T cell differentiation. *Biochim*
824 *Biophys Acta - Gene Regul Mech*. 2016;1859(6):825–831.
825 26. Kim U, et al. The B-cell-specific transcription coactivator OCA-B/OBF-1/Bob-1 is essential
826 for normal production of immunoglobulin isotypes. *Nature*. 1996;383(6600):542–547.
827 27. The GAMES Collaborative Group. Linkage disequilibrium screening for multiple sclerosis
828 implicates JAG1 and POU2AF1 as susceptibility genes in Europeans. *J Neuroimmunol*.
829 2006;179(1–2):108–116.
830 28. Nakamura M, et al. Genome-wide Association Study Identifies TNFSF15 and POU2AF1 as
831 Susceptibility Loci for Primary Biliary Cirrhosis in the Japanese Population. *Am J Hum Genet*.
832 2012;91(4):721–728.
833 29. Sun W, et al. OCA-B/Pou2af1 is sufficient to promote CD4+ T cell memory and
834 prospectively identifies memory precursors. *Proc Natl Acad Sci U S A*.

835 2024;121(9):e2309153121.
836 30. Kim H, et al. Targeting transcriptional coregulator OCA-B/Pou2af1 blocks activated
837 autoreactive T cells in the pancreas and type 1 diabetes. *J Exp Med*. 2021;218(3):133.
838 31. Tzartos JS, et al. IL-21 and IL-21 Receptor Expression in Lymphocytes and Neurons in
839 Multiple Sclerosis Brain. *Am J Pathol*. 2011;178(2):794–802.
840 32. Ndhlovu LC, et al. Critical Involvement of OX40 Ligand Signals in the T Cell Priming Events
841 During Experimental Autoimmune Encephalomyelitis. *J Immunol*. 2001;167(5):2991–2999.
842 33. Hurwitz AA, et al. Cytotoxic T lymphocyte antigen-4 (CTLA-4) limits the expansion of
843 encephalitogenic T cells in experimental autoimmune encephalomyelitis (EAE)-resistant BALB/c
844 mice. *Proc Natl Acad Sci*. 2002;99(5):3013–3017.
845 34. Arellano G, et al. Stage-Specific Role of Interferon-Gamma in Experimental Autoimmune
846 Encephalomyelitis and Multiple Sclerosis. *Front Immunol*. 2015;6(SEP).
847 https://doi.org/10.3389/fimmu.2015.00492.
848 35. Rottman JB, et al. The costimulatory molecule ICOS plays an important role in the
849 immunopathogenesis of EAE. *Nat Immunol*. 2001;2(7):605–611.
850 36. Rouse M, Nagarkatti M, Nagarkatti PS. The role of IL-2 in the activation and expansion of
851 regulatory T-cells and the development of experimental autoimmune encephalomyelitis.
852 *Immunobiology*. 2013;218(4):674–682.
853 37. Duncker PC, et al. GM-CSF Promotes Chronic Disability in Experimental Autoimmune
854 Encephalomyelitis by Altering the Composition of Central Nervous System–Infiltrating Cells, but
855 Is Dispensable for Disease Induction. *J Immunol*. 2018;200(3):966–973.
856 38. Yosef N, et al. Dynamic regulatory network controlling TH17 cell differentiation. *Nature*.
857 2013;496(7446):461–468.
858 39. Ikegami I, et al. Bob1 enhances RORγt-mediated IL-17A expression in Th17 cells through
859 interaction with RORγt. *Biochem Biophys Res Commun*. 2019;514(4):1167–1171.
860 40. Baker D, et al. Autoimmune encephalomyelitis in NOD mice is not initially a progressive
861 multiple sclerosis model. *Ann Clin Transl Neurol*. 2019;6(8):acn3.792.
862 41. Macnair W et al. Single nuclei RNAseq stratifies multiple sclerosis patients into three distinct
863 white matter glia responses. *BioRxiv*. [published online ahead of print: 2022].
864 https://doi.org/https://doi.org/10.1101/2022.04.06.487263.
865 42. Rumble JM, et al. Neutrophil-related factors as biomarkers in EAE and MS. *J Exp Med*.
866 2015;212(1):23–35.
867 43. Kroenke MA, et al. IL-12– and IL-23–modulated T cells induce distinct types of EAE based

868 on histology, CNS chemokine profile, and response to cytokine inhibition. *J Exp Med*.
869 2008;205(7):1535–1541.
870 44. Grifka-Walk HM, Lalor SJ, Segal BM. Highly polarized Th17 cells induce EAE via a T-bet
871 independent mechanism. *Eur J Immunol*. 2013;43(11):2824–2831.
872 45. Schnell A, et al. Stem-like intestinal Th17 cells give rise to pathogenic effector T cells during
873 autoimmunity. *Cell*. 2021;184(26):6281-6298.e23.
874 46. La Manno G, et al. RNA velocity of single cells. *Nature*. 2018;560(7719):494–498.
875 47. Alpsoy A, et al. IκBζ is a dual-use coactivator of NF-κB and POU transcription factors. *Mol*
876 *Cell*. [published online ahead of print: February 24, 2024].
877 https://doi.org/10.1016/j.molcel.2024.01.007.
878 48. Wu XS, et al. OCA-T1 and OCA-T2 are coactivators of POU2F3 in the tuft cell lineage.
879 *Nature*. 2022;607(7917):169–175.
880 49. Schubart DB, et al. B-cell-specif ic coactivator OBF-1/OCA-B/Bob1 required for immune
881 response and germinal centre formation. *Nature*. 1996;383(6600):538–542.
882 50. Qin XF, et al. OCA-B integrates B cell antigen receptor-, CD40L- and IL 4-mediated signals
883 for the germinal center pathway of B cell development. *EMBO J*. 1998;17(17):5066–75.
884 51. Heng TSP, et al. The Immunological Genome Project: networks of gene expression in
885 immune cells. *Nat Immunol*. 2008;9(10):1091–1094.
886 52. Zwilling S, et al. Inducible Expression and Phosphorylation of Coactivator BOB.1/OBF.1 in T
887 Cells. *Science (80-)*. 1997;277(5323):221–225.
888 53. Gearty S V., et al. An autoimmune stem-like CD8 T cell population drives type 1 diabetes.
889 *Nature*. 2022;602(7895):156–161.
890 54. Li Y, et al. Stem-like T cells are associated with the pathogenesis of ulcerative colitis in
891 humans. *Nat Immunol*. [published online ahead of print: June 19, 2024].
892 https://doi.org/10.1038/s41590-024-01860-7.
893 55. Paroni M, et al. Recognition of viral and self-antigens by T H 1 and T H 1/T H 17 central
894 memory cells in patients with multiple sclerosis reveals distinct roles in immune surveillance and
895 relapses. *J Allergy Clin Immunol*. 2017;140(3):797–808.
896 56. Johns TG, et al. Myelin oligodendrocyte glycoprotein induces a demyelinating
897 encephalomyelitis resembling multiple sclerosis. *J Immunol*. 1995;154(10):5536–41.
898 57. Gao Y, et al. Transcription factor EGR2 controls homing and pathogenicity of TH17 cells in
899 the central nervous system. *Nat Immunol*. 2023;24(8):1331–1344.
900 58. McRae BL, et al. Induction of active and adoptive relapsing experimental autoimmune

901 encephalomyelitis (EAE) using an encephalitogenic epitope of proteolipid protein. *J*
902 *Neuroimmunol*. 1992;38(3):229–240.
903 59. Bernard CCA, et al. Myelin oligodendrocyte glycoprotein: a novel candidate autoantigen in
904 multiple sclerosis. *J Mol Med*. 1997;75(2):77–88.
905 60. Anderson AC, et al. A Transgenic Model of Central Nervous System Autoimmunity Mediated
906 by CD4+ and CD8+ T and B Cells. *J Immunol*. 2012;188(5):2084–2092.
907 61. Nish SA, et al. CD4+ T cell effector commitment coupled to self-renewal by asymmetric cell
908 divisions. *J Exp Med*. 2017;214(1):39–47.
909 62. Mammadli M, et al. TCF-1 Is Required for CD4 T Cell Persistence Functions during
910 AlloImmunity. *Int J Mol Sci*. 2023;24(5):4326.
911 63. Kadowaki A, et al. Gut microbiota-dependent CCR9+CD4+ T cells are altered in secondary
912 progressive multiple sclerosis. *Brain*. 2019;142(4):916–931.
913 64. Thakore PI, et al. BACH2 regulates diversification of regulatory and proinflammatory
914 chromatin states in TH17 cells. *Nat Immunol*. [published online ahead of print: July 15, 2024].
915 https://doi.org/10.1038/s41590-024-01901-1.
916 65. Song S, et al. OBF1 and Oct factors control the germinal center transcriptional program.
917 *Blood*. 2021;137(21):2920–2934.
918 66. Sha Y, Markovic-Plese S. Activated IL-1RI Signaling Pathway Induces Th17 Cell
919 Differentiation via Interferon Regulatory Factor 4 Signaling in Patients with Relapsing-Remitting
920 Multiple Sclerosis. *Front Immunol*. 2016;7. https://doi.org/10.3389/fimmu.2016.00543.
921 67. Lane TE, et al. A central role for CD4(+) T cells and RANTES in virus-induced central
922 nervous system inflammation and demyelination. *J Virol*. 2000;74(3):1415–24.
923 68. Blanc CA, et al. Sphingosine-1-Phosphate Receptor Antagonism Enhances Proliferation and
924 Migration of Engrafted Neural Progenitor Cells in a Model of Viral-Induced Demyelination. *Am J*
925 *Pathol*. 2015;185(10):2819–2832.
926 69. Plaisted WC, et al. Remyelination Is Correlated with Regulatory T Cell Induction Following
927 Human Embryoid Body-Derived Neural Precursor Cell Transplantation in a Viral Model of
928 Multiple Sclerosis. *PLoS One*. 2016;11(6):e0157620.
929 70. Dickey LL, et al. MicroRNA-155 enhances T cell trafficking and antiviral effector function in a
930 model of coronavirus-induced neurologic disease. *J Neuroinflammation*. 2016;13(1):240.
931

Hughes et al. Figure 1

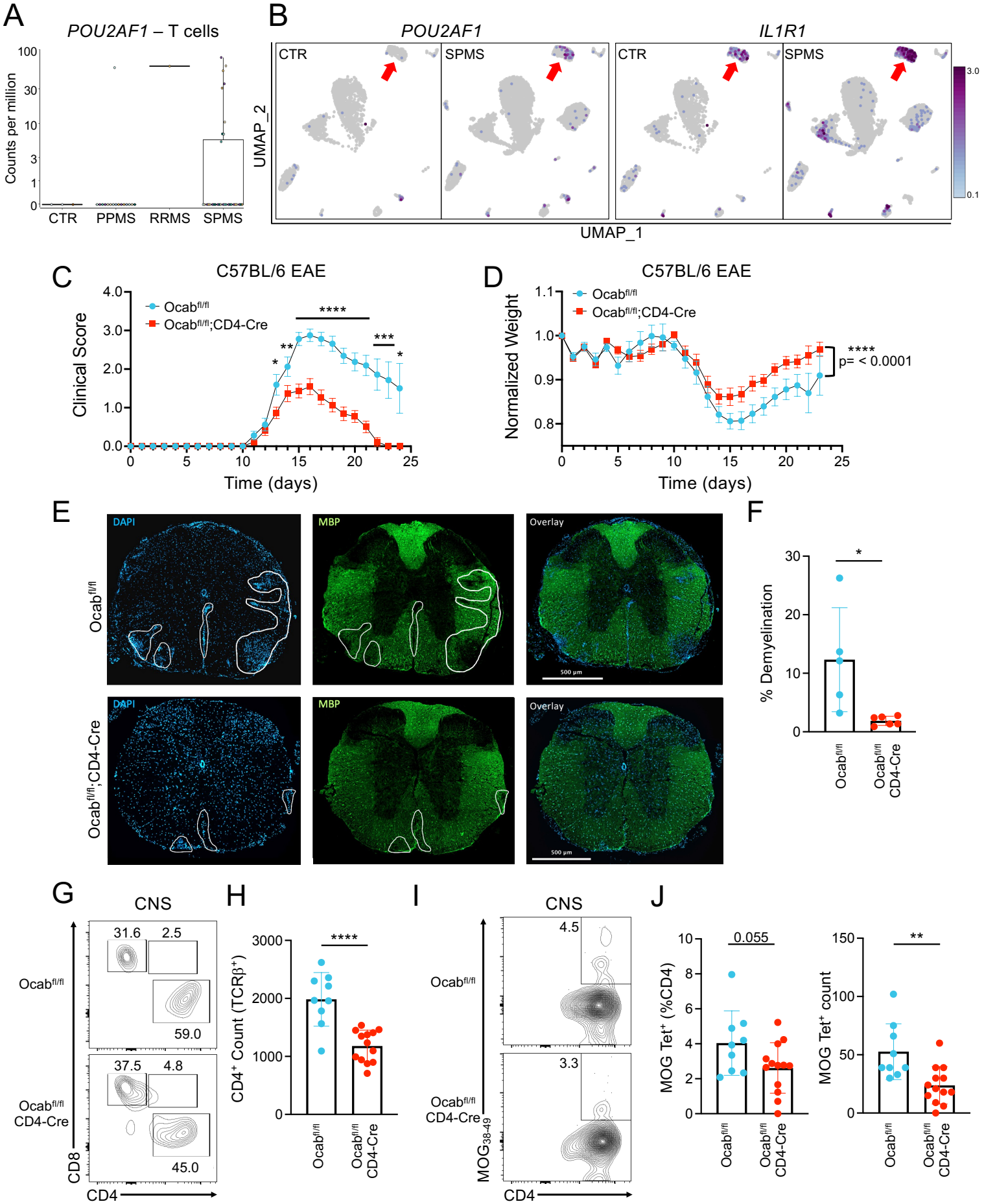

Hughes et al. Figure 2

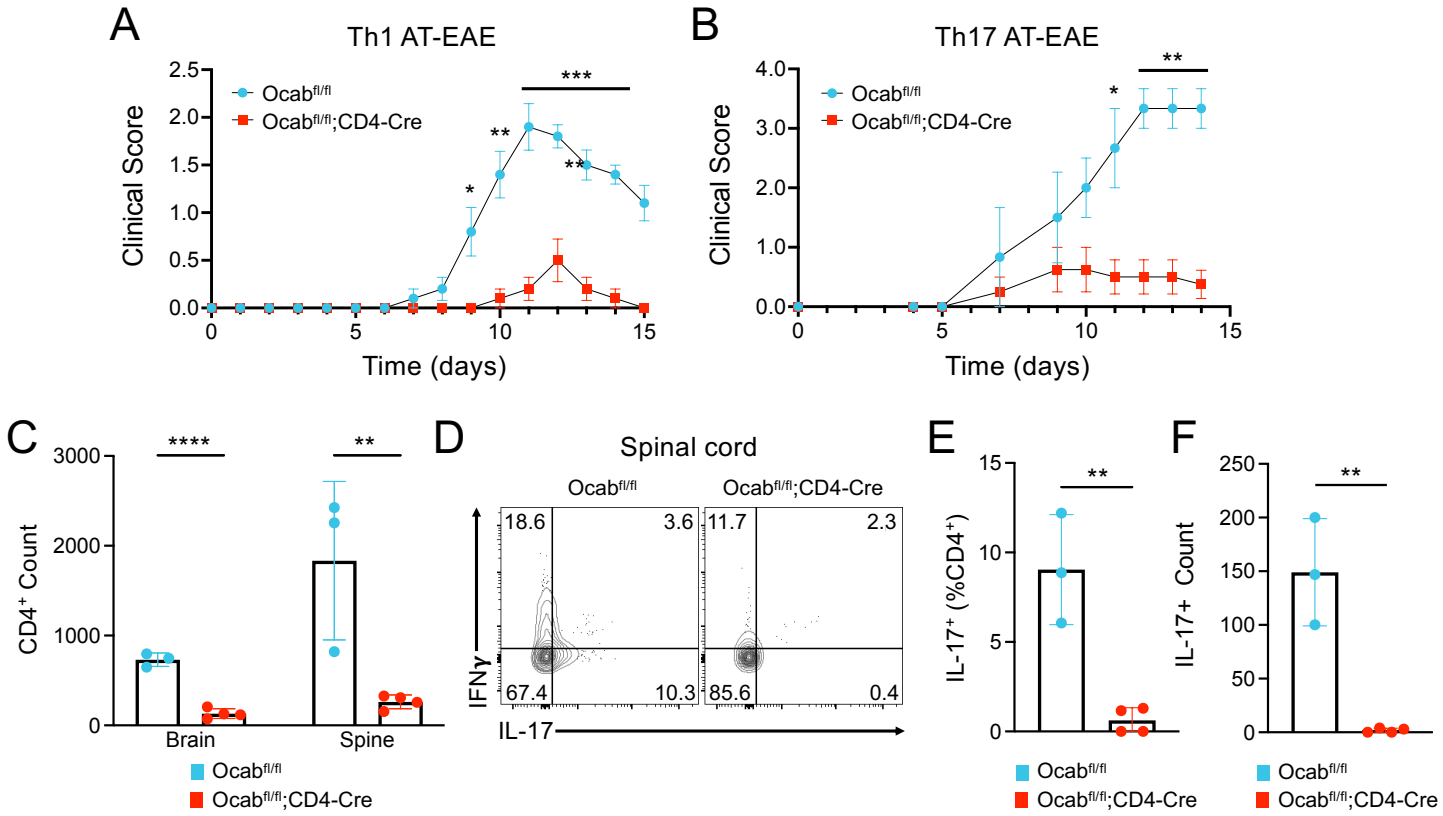

Hughes et al. Figure 3

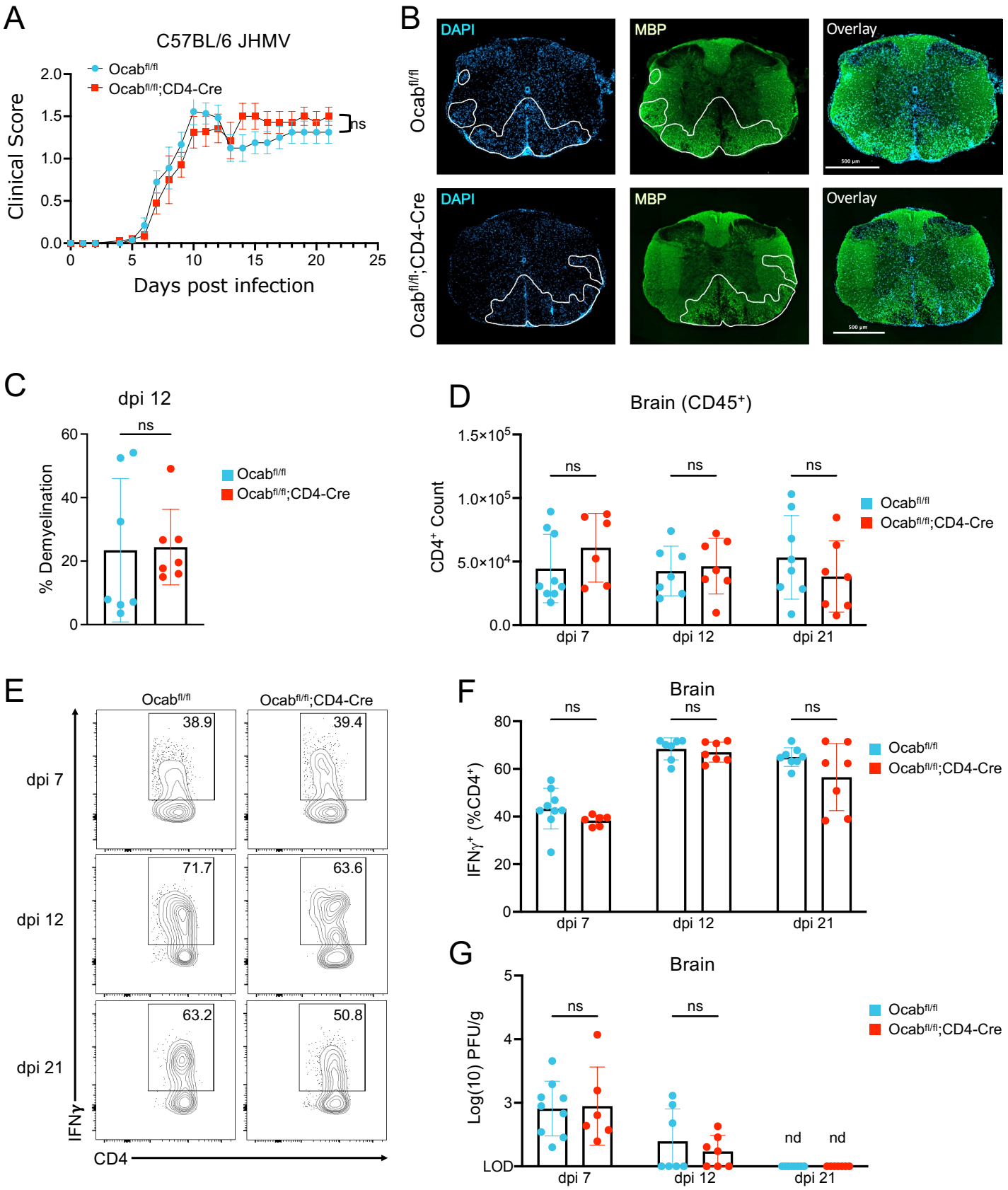

Hughes et al. Figure 4

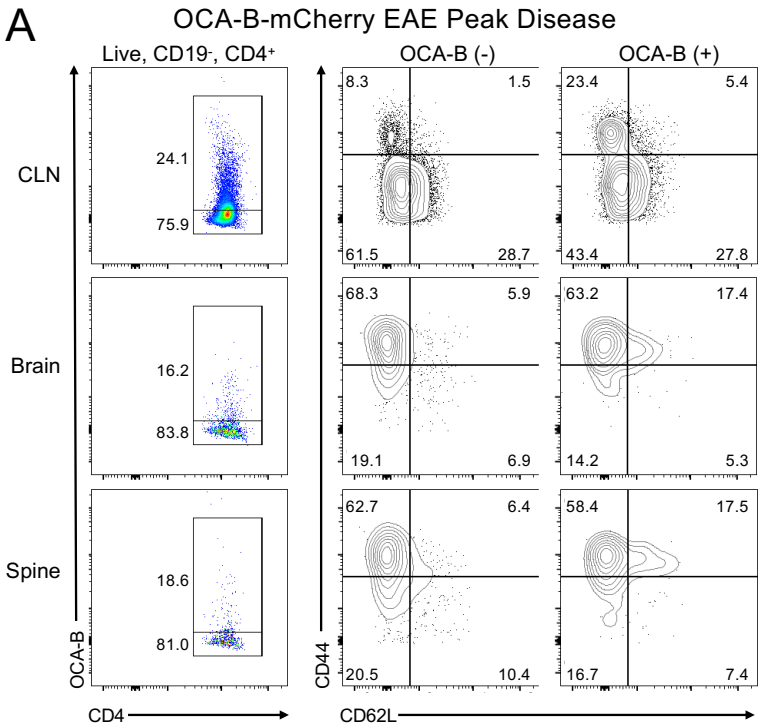

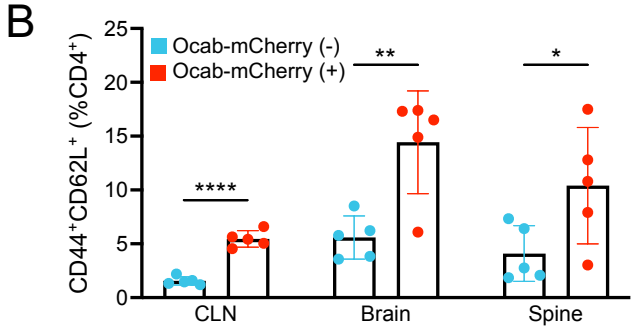

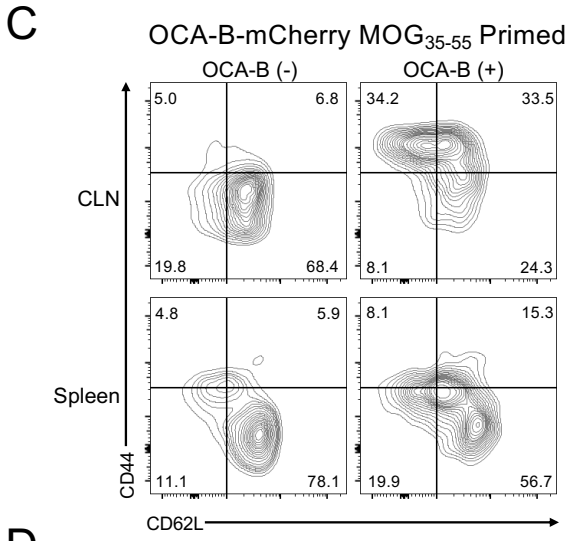

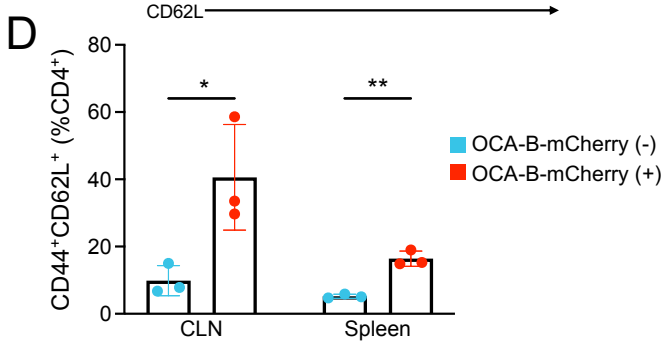

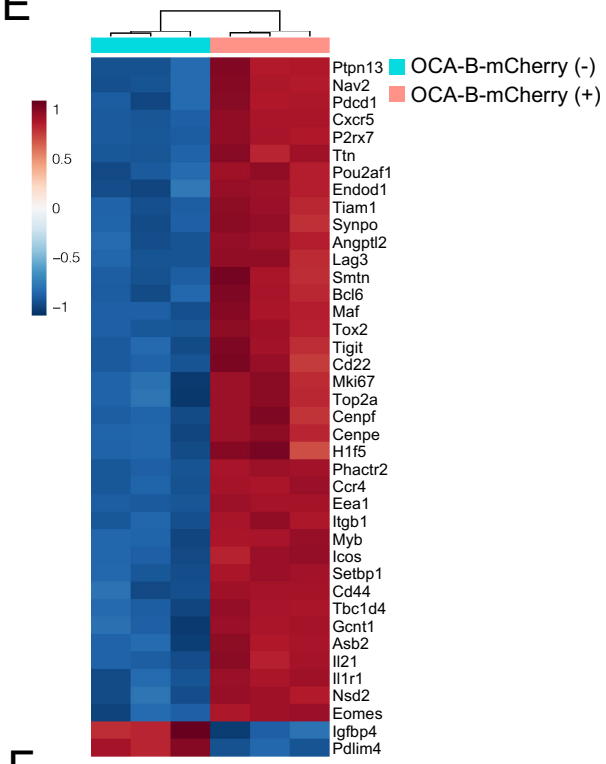

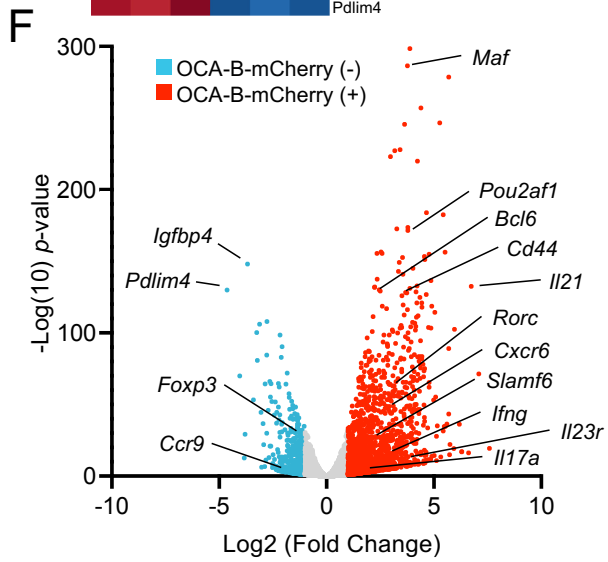

G

OCA-B+ Enriched Pathways

KEGG Pathway	*p*-value
Systemic Lupus Erythematosus	1.02E-04
Cytokine Cytokine Receptor Interaction	5.04E-04
Autoimmune Thyroid Disease	1.16E-03
Type I Diabetes Mellitus	2.06E-03

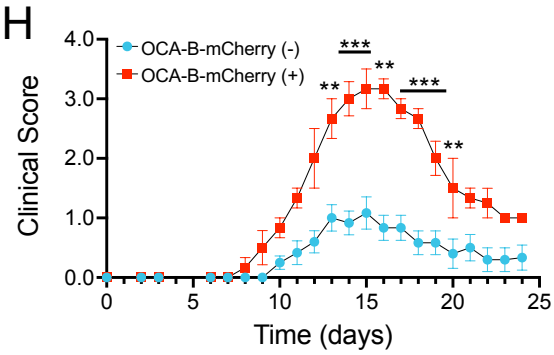

Hughes et al. Figure 5

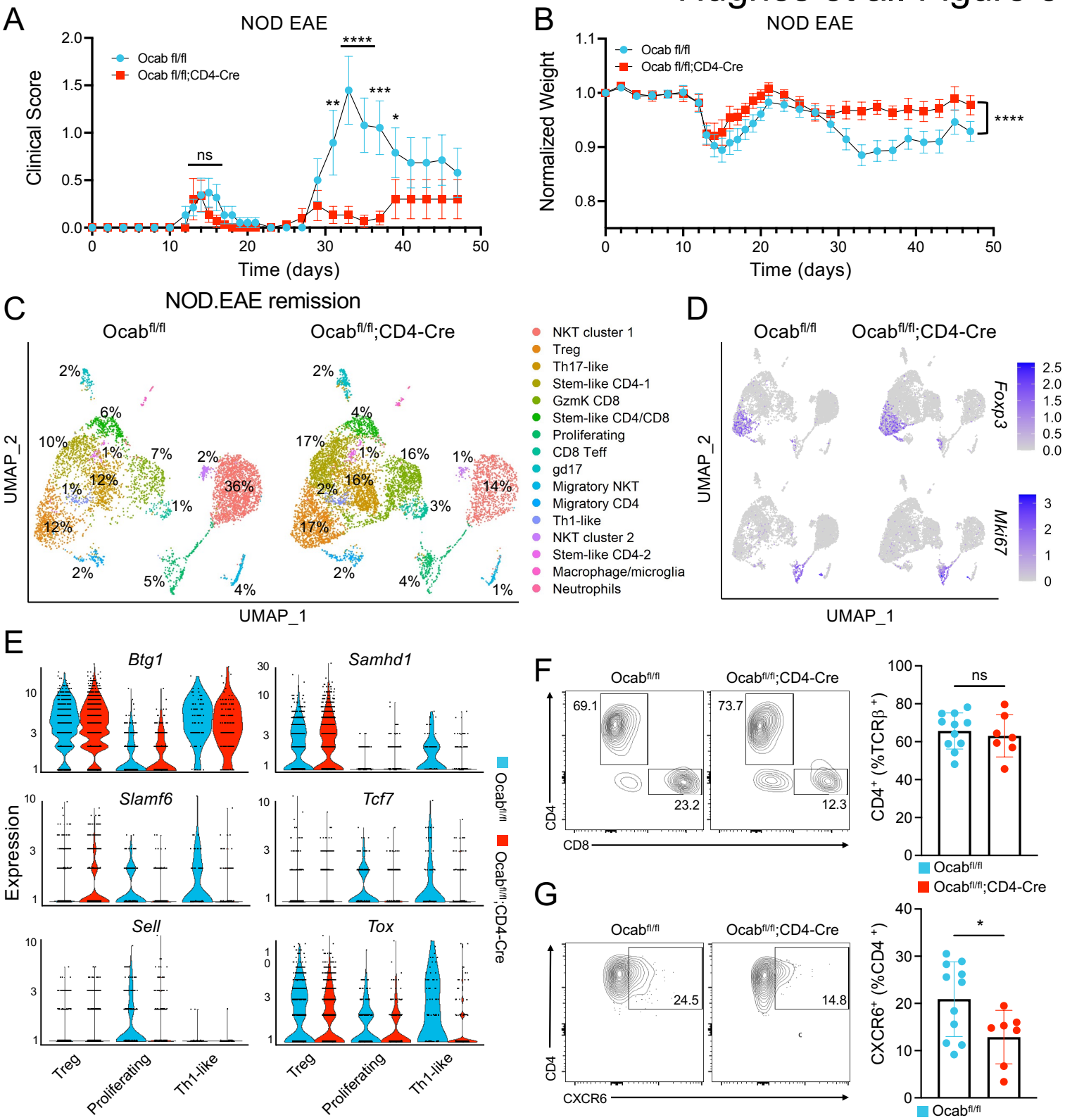
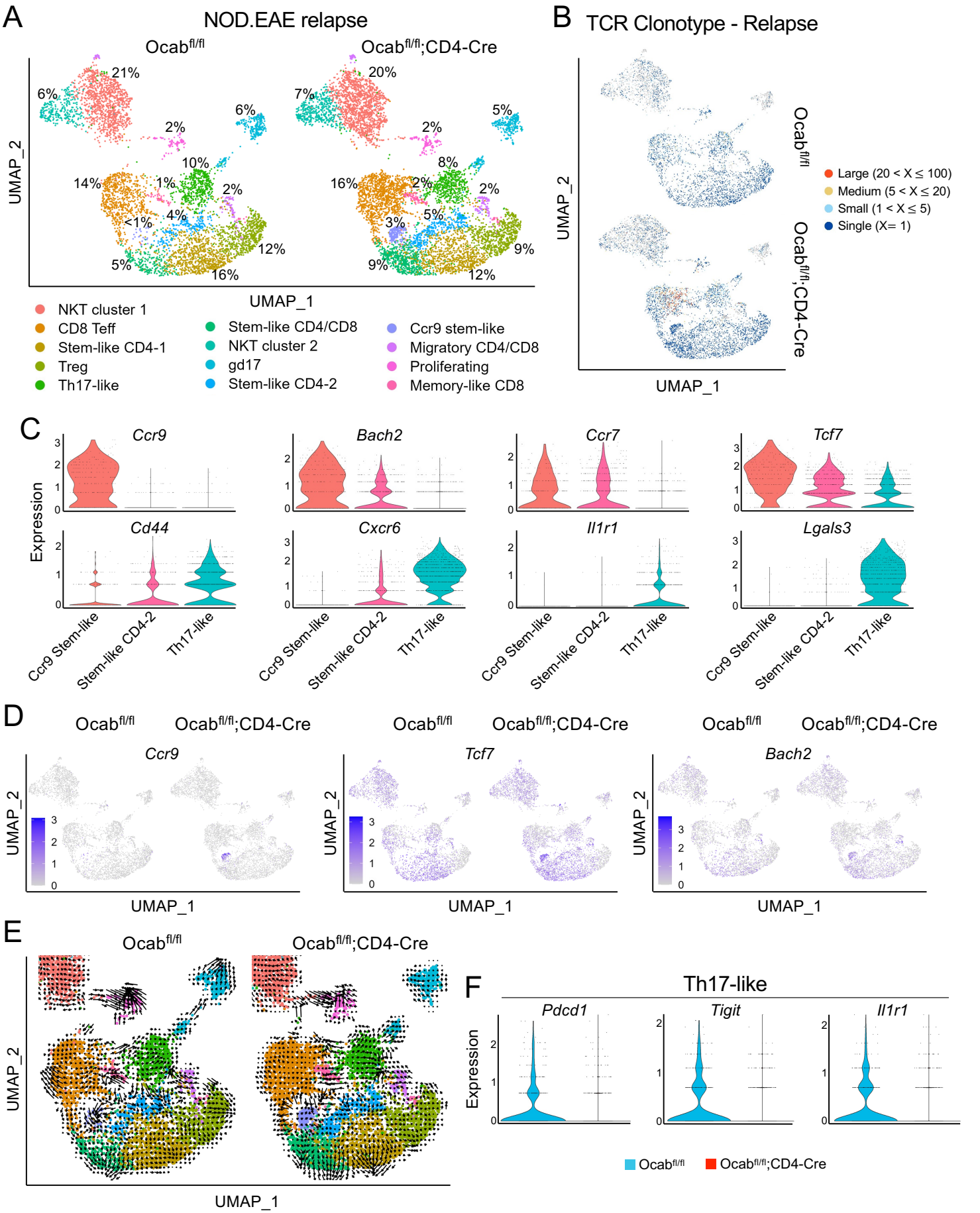
Hughes et al. Figure 6